Technical Report...

ADVANCED FERRIMAGNETIC MATERIALS
APPLIED TO DIGITAL PHASE SHIFTERS

FIRST SEMIANNUAL REPORT

25 June 1964 to 25 December 1964

ARPA ORDER NO. 550
PROGRAM CODE NO. 4730

RADC CONTRACT NO. AF30(602)-3449

DDC

FEB 0 , 1965

DDC-IRA B

Air Force Systems Command
Research and Technology Division
Rome Air Development Center
Griffiss Air Force Base, New York

Project Defender
Advanced Research Projects Agency (ARPA)
Department of Defense
Washington, D.C.

(SPERRY) MICROWAVE ELECTRONICS COMPANY

CLEARWATER FLORIDA

TECHNICAL REPORT

ADVANCED FERRIMAGNETIC MATERIALS APPLIED

to

DIGITAL PHASE SHIFTERS

FIRST SEMIANNUAL REPORT

25 June 1964 to 25 December 1964

ARPA ORDER NO. 550

PROGRAM CODE NO. 4730

RADC CONTRACT NO. AF30(602)3490

Prepared for:

Air Force Systems Command
Research and Technology Division
Rome Air Development Center
Griffiss Air Force Base, New York

and

Project Defender
Advanced Research Projects Agency (ARPA)
Department of Defense
Washington D.C.

Title of Work: Investigation directed toward the improvement and
evaluation of ferrimagnetic materials for use in
microwave digital phase shifters at L-, S-, C-,
and X-bands.

January 1965

SPERRY MICROWAVE ELECTRONICS COMPANY
DIVISION OF SPERRY RAND CORPORATION
CLEARWATER, FLORIDA

SJ. M 220-0052-3   Copy No. 26

TABLE OF CONTENTS

BLANK PAGE

LIST OF ILLUSTRATIONS

1. SYNOPSIS

This is the first Semiannual Report on this program. The objectives and responsibility of the program are outlined in the first section of this report.

The operating characteristics of microwave ferrite digital phase shifters and the dependence of these characteristics on material parameters are discussed. The importance of the following material parameters are covered:

- Saturation magnetization $4\pi M_s$
- Remanent magnetization $4\pi M_R$
- Linewidth ΔH
- Remanence ratio $4\pi M_R / 4\pi M_s$
- Coercive field
- Density
- Grain size
- Dielectric constant
- Dielectric loss tangent
- Anisotropy field
- Peak power threshold

The experimental investigations on materials to date have concentrated on the hybrid garnet compositions. Compositions comprised of individual and composite substitutions of the following metal ions in yttrium iron garnets have been prepared and evaluated: gadolinium, holmium, dysprosium, erbium, terbium, samarium, ytterbium, aluminum, and gallium. The structural, microwave, and magnetic characteristics of these compositions have been tabulated. The influence of the preparation procedure parameters on the properties of the materials are described.

Conclusions are offered in regard to the material characteristics tabulated with additional interpretation on structural effects.

Rf evaluation of some of the materials has been performed in X-band waveguide. The results of these investigations are discussed.

2. INTRODUCTION

2.1 BACKGROUND OF PROGRAM

Investigators in the field of microwave devices have attempted for several years to derive high performance, low cost, fast acting components which require low switching and holding power for fast scanning array applications. The development of microwave devices utilizing the square hysteresis loop properties of ferrimagnetic materials seems to be a very promising approach toward these components. These fast switching microwave devices require toroidal material geometries with the cores magnetized circumferentially. The toroidal materials are to possess excellent microwave characteristics as well as square hysteresis loops; that is, large values of remanent magnetization and low coercive fields.

One fast switching device in this category is the ferrite digital phase shifter. These devices utilize toroidal cores for phase shifting elements and are switched in very much the same fashion as computer cores. The operating characteristics of these digital phase shifters depend to a great extent on the properties and availability of acceptable ferrimagnetic materials. While the structural configurations of the rf portion of the phase shifter are still under development and many new configurations are constantly being generated, in most every case the properties of the desired ferrimagnetic materials are quite similar. Therefore, it is very important to have a number of very suitable and optimized materials for utilization in these phase shifters. It is the purpose of this program to derive a number of optimized materials for utilization in digital phase shifters operating from L through X band and to further demonstrate their usefulness by evaluation in rf structures.

2.2 PROGRAM OBJECTIVES

The objectives of this program are directed toward the improvement and evaluation of ferrite and garnet materials for use in digital phase shifters at L, S, C and X bands. Emphasis is to be placed on peak power capability exceeding 10 kilowatts and phase stability with temperature variation over the military range. Microwave digital phase shifter structures will be studied with special emphasis placed upon the materials derived in this program combined with the requirements for high switching speed, low switching power, low loss, low holding power, compact configurations, low cost per unit and high peak and average power handling capabilities. Eighty percent of the effort will be directed toward the materials study and evaluation.

2.3 ASSIGNMENT OF RESPONSIBILITY FOR THE PROGRAM

This program is assigned to the Engineering Department of the Sperry Microwave Electronics Company. Dr. R. E. Henning is the Chief Engineer. The program responsibility is in the Microwave Equipment Department with Mr. B. J. Duncan, Engineering Manager. The Project Engineer responsible for the program is Dr. G. R. Harrison, Research Section Head. The material investigations or the program are being conducted by Mr. L. R. Hodges, Senior Staff Engineer and Mr. L. A. Crouch, Senior Engineer. The microwave digital phase shift structures and the rf evaluation of the materials are directed by Mr. Julian Brown, Engineering Section Head. The structural investigations are being carried out by Mr. D. R. Taft, Senior Staff Engineer.

3. DISCUSSION OF MATERIAL CHARACTERISTICS

3.1 GENERAL

The ferrite digital phase shifter (FDPS) is a device which requires toroidal material geometries (cores or tubes). The toroids are magnetized circumferentially.

Ferrimagnetic digital phase shifters make use of several of these toroidal "cores" of ferrimagnetic material installed along the longitudinal axis of rectangular waveguide or coax transmission line. The location is such as to cause the propagating waves to be coupled to the cores in a reciprocal or nonreciprocal manner. The toroidal cores are composed of a very high performance microwave material and to achieve reasonable digital action, must exhibit a square or near square hysteresis loop. The two remanent states of magnetizations are the normal operating positions. In the digital phase shifter designs, each core is supplied with a circumferential applied magnetic field which is used to switch the magnetization within it. The difference in permeability realized between the two remanent states of magnetization yields a differential phase shift proportional to the core lengths and the material properties. The lengths of the cores are selected in accordance with digit requirements; for example, with 360° of phase shift required, one core or tube each may be provided to yield 180°, 90°, 45°, 22.5^O, 11.25^O and 5.625^O. The result will be a phase shifter capable of exhibiting any differential phase shift from 0° to 360° in 5.625^O steps. Common terminology is to call this phase shifter a six-digit or six-bit phase shifter.

For nonreciprocal phase shifters the structure is such that a portion of a magnetized toroid will see a circular (or elliptical) polarized rf magnetic field of one sense (positive or negative) for one direction of magnetization. Switching the direction of magnetization in the toroid reverses the sense of the circular polarized incident rf magnetic field and thus produces a differential phase shift. Accordingly, for one direction of magnetization of any given toroid, a prescribed phase shift will be obtained and, for the opposite direction, a different value will be evident. The lower value can be used as a "zero" base. Since the toroidal core exhibits a nearly square hysteresis loop, a current pulse (large enough to produce a magnetic field somewhat greater than the coercive field of the material) is used to switch the magnetization after which the magnetization falls into the remanent state and holds (no holding current is required). The circumferential switching field is generated by passing a current pulse through a turn of wire which threads the core.

The material configuration and characteristics for reciprocal operation are essentially identical to the nonreciprocal case.

The operating characteristics of the FDPS are heavily dependent on the properties of the ferrimagnetic material utilized as detailed in the following sections.

3.2 OPERATING CHARACTERISTICS

No attempt will be made to present a rigorous mathematical interpretation of the interaction characteristics of ferrimagnetic toroidal materials and rf signals. A physical interpretation will be presented to indicate the mechanisms involved.

In an unmagnetized domain-filled ferrimagnetic material called "low field" magnetic losses have been predicted and experimentally verified to be present out to a maximum frequency given by

$$\omega_{(max)} = \gamma \left[H_{anis} + 4\pi M_s \right] \tag{1}$$

where

$\omega_{(max)}$ = maximum frequency (mHz) for low field magnetic losses (no applied field)

γ = gyromagnetic ratio (mHz/oersted)

γ $\approx$ 2.8 mHz/oersted for most materials

H_{anis} = anisotropy field (oersteds) of the material

$4\pi M_s$ = saturation magnetization (gauss) of the material

This equation has been derived by consideration of internal demagnetizing fields[1] and from Kittel's resonance equation[2] (macroscopic magnetization considerations) together with internal demagnetizing fields associated with domains. This relationship indicates that resonance losses in the absence of an applied field (unmagnetized sample) will be observed to a maximum frequency as predicted by equation (1).

[1] D. Polder and J. Smit, "Resonance Phenomena in Ferrites," Rev. Modern Phys., 25, 89 (1953)

[2] B. Lax and K. J. Button, Microwave Ferrites and Ferrimagnetics, McGraw-Hill Book Company, New York, 1962, pp. 444-450

For toroidal geometries where a material possesses a very high remanence ratio (high value of remanent magnetization) the material will be nearly magnetized (very few domains). In this situation there is no applied field in accordance with the case of low field losses discussed above. If an rf field is applied which is perpendicular to the magnetization, the broad distribution of loss as shown in curve A of Figure 1 is confined to a resonance peak similar to that shown in B of Figure 1. This type of response is very similar to ferrimagnetic resonance and obeys similar, established permeability relationships for ferrimagnetic materials at microwave frequencies.
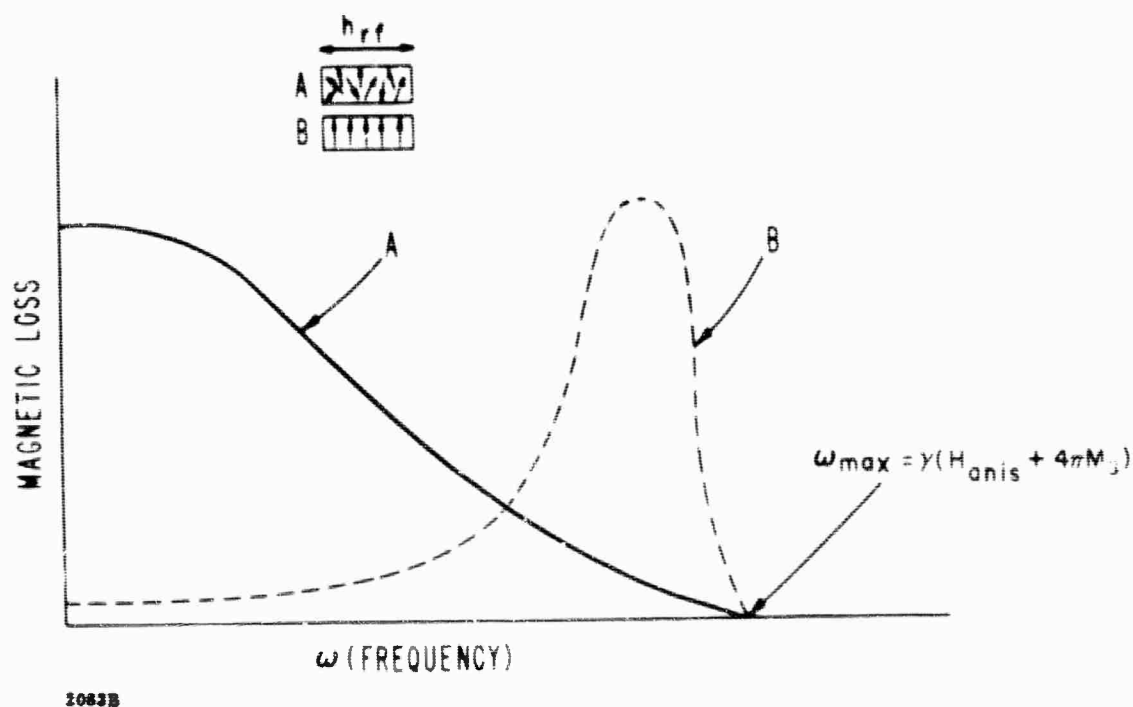
Figure 1. Low Field Losses in Ferrimagnetic Materials

The frequency at which this resonance occurs appears to be formulated as follows:

$$\omega = \gamma\, 4\pi M_R \tag{2}$$

where $4\pi M_R$ is the remanent magnetization in gauss of the material.

This expression does not follow from Kittel's resonance equation using geometrically computed demagnetizing factors. Since the low field loss mechanisms are essentially confined to a narrow frequency region, it follows that this frequency region will be somewhat less than that predicted by equation (1). Single domain resonance arguments from Kittel's resonance equation indicate that this resonance should occur at [3]

$$\omega = \gamma\left(\frac{4\pi M_S}{2}\right) \tag{3}$$

where $4\pi M_S$ is the saturation magnetization in gauss.

Experimental results indicate, however, that equation (2) is more appropriate for use in predicting the resonance frequency for the toroidal geometries normally employed in ferrite digital phase shifters[.] This relationship is important to the design of phase shifters. The phase shift is proportional to the magnetization but, as indicated here, so are the magnetic losses. Therefore the choice of magnetization used for a given frequency must be such as to produce ample phase shift per unit length and also to place the point of operation out of the magnetic loss region as predicted by equation (2). For a given frequency of operation the value of $4\pi M_S$ utilized in FDPS is generally in the region of $1/3$ to $2/3$ of the value predicted by equation (2) for resonance at that frequency. The value of the magnetization of the material determines the point of operation in these devices in a similar fashion as the dc applied magnetic field for normal ferrite devices.

The values of the remanent and saturated magnetization are therefore very important to the choice of a material for FDPS.

The value of the remanence ratio $\left(R_R = \dfrac{4\pi M_R}{4\pi M_S}\right)$ indicates the degree of unfavorably oriented domains and to this extent affects the shape and width of the resonance absorption curve. High remanence ratio will better confine the absorption peak such as curve B in Figure 1; low remanence ratio will produce lower absorption and broader width with appreciable low frequency skirts.

[3] B. N. Enander, "A New Ferrite Isolator", Proceedings of the IRE 4,4, 1421 (October, 1956).

This brings up the question of the importance of ferromagnetic resonance linewidth to the operation of digital phase shifters. The linewidth is normally measured on spherical samples with an applied field in accordance with the equation

$$\omega = \gamma H_{app} \tag{4}$$

where H_{app} is the applied dc field in oersteds.

The resonance characteristics per equation (2) are without doubt much broader than that measured in the usual sense as per equation (4). The normally measured linewidths on spheres will influence the selection of materials for application in digital phase shifters; however, the criterion for this selection is not presently established. Since the "so-called" linewidth in digital phase shifter geometries is influenced by remanence ratio, additional analysis must be performed to specify optimized materials as far as linewidth is concerned.

Other material parameters which must be discussed in regard to FDPS are dielectric constant, dielectric loss tangent, coercive fields, density, grain size and peak power thresholds.

Dielectric loss tangents of acceptable materials should be as low as possible. Values in the range of 0.0001 or less as measured at X band are desirable.

Dielectric constants of most any value are acceptable but should be reproducible. The dielectric constant of the material will affect the structural configuration and the match of the phase shifter. Any variation in dielectric constant on a reproducible basis will affect the length of material required to achieve a given phase shift and therefore would influence the degree of difficulty and cost in producing phase shifters in large quantities.

Each of these material parameters will be discussed in detail in the following sections.

3.3 REMANENCE RATIO

There is no general agreement as to the shape a hysteresis loop should have to be to be called square. A "squareness ratio"[4] as defined for computer applications has no useful meaning for the above microwave applications; for most ferrimagnetic materials this parameter is maximum for minor hysteresis loops as used in computers and is generally zero or near zero for the saturated loop.

The most useful parameter related to the loop is the saturated remanence ratio defined as

$$R_R \; = \; B_R/B_S \; \approx \; \frac{4\pi M_R}{4\pi M_s} \tag{5}$$

where B_R and $4\pi M_R$ are the remanent induction and magnetization respectively of the loop (See Figure 2) and B_S and $4\pi M_s$ are the induction and magnetization respectively at saturation.

The remanence ratio should be as near unity as possible. The operating point and thus the characteristics of the microwave device are dependent on the value of $4\pi M_R$.

In a polycrystalline ferrite or garnet the intrinsic magnetization in the individual crystals (cubic) prefers to be in the so called easy direction. The easy directions are determined by the magnetocrystalline anistropy, the stress anisotropy (magnetostriction), and the shape anisotropy . If such a material has only magneto-crystalline anisotropy, the remanence ratio can be calculated to be 0.87. This result assumes that in the saturated state the magnetization in all crystals is parallel to the applied field and relaxes to the nearest easy direction (this direction is along the body diagonal, the 111 axis in cubic materials with negative anistropy) when the field is removed. This ideal value sometimes is difficult to obtain because of the unfavorable contributions of the other anisotropies.

A unidirectional anisotropy can sometimes be built into the material by controlling the stress and shape of the material, thus producing higher values of the remanence ratio. Quenching, lattice deformations, applied pressure, etc., are techniques sometimes used.

------

[4] J. B. Birks and J. Hart, Progress in Dielectrics, Vol. 5, Academic Press Inc., Publishers, New York, 1963. (H. P. Peloschek, "Square Loop Ferrites and Their Applications", pp 37-93).
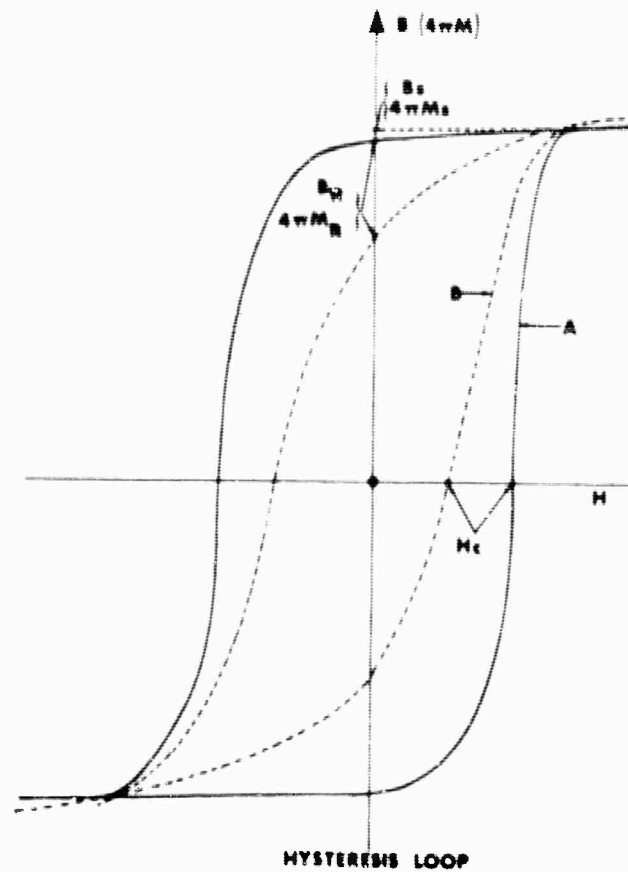
Figure 2.   Hysteresis Loops of High (A) and Low (B) Remanence Materials

High remanence ratios can be obtained if the magnetocrystalline anisotropy is large 'n comparison to the other anisotropies.   This implies low magnetostriction, low unfavorable internal stresses, and a dense homogeneous material (high density).

In microwave applications the resonance linewidth and shape which are dependent on the remanence ratio will be most favorable and applicable for those materials possessing high remanence ratios.

The remanence ratio depends primarily on the composition, method of preparation grain size, and homogeneity of the material[4].

---

[4]Ibid. , p. 3-6

3.4 COERCIVE FORCE

The coercive force (H_c) of the material is another very important parameter of the hysteresis loop (see Figure 2). Acceptable materials for most applications demand low coercive fields to minimize power consumption. For low coercive force, a dense chemically and structurally homogeneous material is required with anisotropy fields as low as possible. The coercive force seems most greatly affected by composition, grain size and porosity.

3.5 SWITCHING POWER

The switching power required depends primarily on material parameters. Excluding external circuit losses, the power consumed in switching a ferrite core is (assuming a square hysteresis loop):

$$P \text{ (watts)} = 4H_c (M_R) \, V R \times 10^{-7} \tag{6}$$

where

H_c = coercive field of material in oersteds

M_R = remanence magnetization in gauss

V = volume of sample in cm^3

R = switching rate in cycles/second

This equation implies that, from a switching power standpoint, H_c should be as small as possible. The value of the remanent magnetization should be as low as possible, compatible with the desired operating characteristics. The size (volume) of the toroid should be structurally as small as possible.

It is generally more desirable to specify switching energy rather than power for comparison of materials. This removes the ambiguity of switching rate from the above equation.

$$\text{Switching energy (} \mu\text{joules)} = 0.4 H_c (M_R) \, V \tag{7}$$

For a general rule of thumb in computing total energy or power required for switching, the external circuit losses can be assumed to be approximately equal to the energy expended in the core. Circuit losses however can be controlled to a great measure by the ingenuity of the investigator and/or structural compatibility. Experimental data indicate that in general these losses can be reduced to values of the order of the core losses.

3.6 SWITCHING TIME

The switching time depends on the speed at which domain walls may be moved in the material. This is the predominant magnetization process for switching the direction of magnetic moments in the core. The domain wall velocity is given by:[5]

$$\nu = \frac{15.7\, \delta\, g^2\, M_s}{\lambda}\, (H_{app} - H_c) \tag{8}$$

For $H_{app} \ll 4\pi M_s$

$\quad \nu$ = the velocity in cm/sec

$\quad \delta$ = the domain wall thickness (cm)

$$\delta \approx \sqrt{\frac{k\, T_c}{K_1\, a}} \tag{9}$$

$\quad k$ = Boltzmann's constant

$\quad T_c$ = Curie temperature of the material (^{0}K)

$\quad K_1$ = first order anisotropy constant (ergs/cm^3)

$\quad a$ = lattice constant of the material (cm)

$$K_1 = \frac{H_{anis}\, M_s}{2}\ (ergs/cm^3) \tag{10}$$

$\quad H_{anis}$ = anisotropy field of the material (oersteds)

$\quad M_s$ = saturation magnetization (gauss)

$\quad g$ = g-factor (for Equation 8 in cycles/oe-sec)

$\quad H_{app}$ = applied switching field (oersteds)

$\quad H_c$ = coercive force (oersteds)

$\quad \lambda$ = damping parameter (sec^{-1})

---

[5] C. L. Hogan, unpublished notes, Harvard University, Cambridge, Mass.

$$\lambda \approx \frac{\gamma M_s \, \Delta H}{2 \, H_r} \tag{11}$$

ΔH = linewidth of material (oersteds)

H_r = field required for ferrimagnetic resonance (oersteds)

γ = 1.4 g-factor (cycles/oe-sec)

Switching time is therefore:

$$t = \frac{d}{\nu} \tag{12}$$

where d is the average distance the domain wall must move.

d is proportional to the type material, preparation procedure, grain size and geometry of sample. Switching time is related to the above parameters as:

$$t \approx \frac{6.4 \, d \, \lambda \times 10^{-2}}{\delta g^2 \, M_s \, (H_{app} - H_c)} \tag{13}$$

This equation implies that the switching time is dependent largely on material parameters.

For fast switching time, the domain dimensions, H_{anis}, M_s and ΔH of the material, should be as small as possible. The Curie temperature and switching field should be as large as feasible.

It is important to note here that, as the toroids are switched, H_{app} drives the domain walls, and thus this time may be very fast. However, when the cores have been driven to saturation, H_{app} is removed and the core is allowed to fall into the remanent state. This "fall back" time may be much longer, particularly if $4\pi M_R$ is much less than $4\pi M_s$ since there is normally no driving field for domain walls except the demagnetizing fields.

It is important, therefore, for the material to possess a $4\pi M_R / 4\pi M_s$ ratio as high as possible. A material possessing a hysteresis curve such as "A" in Figure 2 is therefore preferred over that of "B".

Switching energy for a typical core is in the 80 to 200 μjoule region, depending on the specific material characteristics. Domain wall velocities are typically in the 10^3 to 10^4 cm/sec region and feasible switching times are in the region of 0.5 to 2 μsec for nominal power consumption. Switching rates are now feasible up to the 100 kc region.

Switching times much faster than that indicated are certainly feasible from a mechanism standpoint. Equation (13) indicates that for a given material the switching time is inversely dependent on the switching field which is directly proportional to switching power. Therefore, switching times in the nanosecond region are certainly feasible from a mechanism analysis; however, this is achieved at the expense of drive power.

Equation (12) implies that switching time is directly proportional to the distance domain walls must move. It should be mentioned that domain rotation is certainly a possible magnetization process in addition to that of domain wall motion. Domain walls are much easier to move for nominal switching times and power. This is therefore the dominant process for reversing the magnetization in toroidal cores. It is possible that the switching pulse could be too fast or short to interact with domain walls. For very fast switching pulses of sufficient energy content, domain rotation may become the dominant magnetization process. In this mode of magnetization the coercive field of the material appears to be much larger than for domain wall motion; therefore, much more energy is required to switch the core.

Since domain wall motion is the most desirable mode of switching, it is important to nucleate many walls rapidly and once nucleated, to move the walls with the least resistance (minimum applied energy). Walls have a tendency to cling on inclusions, pores and imperfections in the grains. Grain density or sample density therefore should be as high as feasible. Grain sizes capable of containing multi-domains are preferred over single domain particles.

As grain size is reduced, a critical size is reached whereby the grain can contain only a single domain. This size is dependent on material parameters in accordance with the following expression[5]:

$$ R_c = \frac{9H_{anis}}{4\pi M_s}\delta \approx \frac{9H_{anis}}{4\pi M_s} \sqrt{\frac{2k\,T_c}{H_{anis}\,M_s\,a}} = \frac{9}{4\pi M_s} \sqrt{\frac{2k\,H_{anis}\,T_c}{M_s\,a}} \quad (14) $$

[5] C. L. Hogan, unpublished notes, Harvard University, Cambridge, Mass.

There re

$$R_c \sim \frac{\sqrt{K_1}}{M_s^2}$$

(15)

where

R_c = critical radius (cm)

H_{anis} = anisotropy (oersteds)

M_s = saturated magnetization (gauss)

δ = domain wall thickness (cm)

T_c = curie temperature of the material (^{o}K)

a   = lattice constant of the material

K_1 = first order anisotropy constant (ergs/cm^3)

This expression predicts a value of approximately 0.1 microns (0.2 microns grain size) for yttrium iron garnet; for materials with lower magnetization. the critical radius would be larger (up to the 1 micron region).

When the average grain size is reduced below this critical value, domain rotation must be used as the dominant magnetization process. Such materials generally possess very high coercive fields.

As grain size is increased, multi-domains may exist in each grain and if each grain is homogeneous and relatively free of imperfections, the domain walls thus generated are easily moved (low coercive fields). When each grain is magnetized, the unfavorable domains required to reach the remanent state of magnetization will primarily nucleate initially at the grain surface. As grain size increases, the surface-to-volume ratio decreases. Lower surface-to-volume ratio implies proportionally fewer unfavorable domains; therefore the remanence ratio increases. However, each grain is capable of containing multiple domains, which is advantageous for fast switching with minimum power.

Remanence ratios, therefore, are expected to be higher and the coercive fields lower for materials possessing an average grain size much larger than the critical radius. Experimental evidence verifies this conclusion; in fact, the larger the grain size the more favorable are the hysteresis properties for digital phase shifter applications.

3 12

3.7 HIGH POWER CHARACTERISTICS

The performance of digital phase shifters operating below ferromagnetic resonance will deteriorate under the application of sufficiently high microwave power levels. By analyzing the cause of this degradation in performance, the properties of materials used in digital phase shifters can be tailored to permit satisfactory operation up to very high peak power levels (100 kw or more). The onset of high power effects in ferrite phase shifters is evidenced by an abrupt increase in insertion loss when the rf power exceeds a certain critical value. As a result of this increase in power absorbed, local regions of the materials are heated and the saturation magnetization may decrease if the material magnetization has a sufficiently strong dependence on temperature. Local demagnetizing fields may then be created which cause the entire toroid to assume lower remanence ratio and the observed phase shift is thereby decreased.[6] By increasing the threshold power level for the onset of high power absorption, the degradation in phase shift can be avoided.

Suhl[7] and Schlomann[8] have both treated high power effects in ferrites in considerable detail, and have shown these effects to arise from the build up of oscillations of pairs of spin waves whose frequencies are degenerate with the applied microwave frequency or equal to one half the operating frequency. The half frequency spin waves are more closely coupled to the uniform precession of the magnetization than are the degenerate spin waves. Thus the diversion of energy from the uniform precession to the half frequency spin waves is called a first order process, while the coupling to degenerate spin wave is termed second order.

The second order process has a lowest threshold when the material is biased to resonance and results in a saturation of the main resonance absorption line at high power levels. Since digital phase shifters are always operated far from resonance, this second order process is of little importance here.

The first order process (energy scattering to half-frequency spin waves) may occur when the material is biased to resonance, or it may be observed as an anomalous absorption below the field required for resonance. Since phase shifters are

[6] H. Hair, Final Report, Subcontract #250, Prime Contract No. AF-19(628)-500 Prepared for MIT Lincoln Laboratories by the Heavy Military Electronics Department, G.E., Syracuse, N.Y. (Dec. 1964)

[7] H. Suhl, J. Phys. Chem. Solids $\underline{1}$, 209 (1957)

[8] E. Schlomann, J.J. Green and U. Milano, J. Appl. Phys. $\underline{31}$, 3945s (1960)

normally operated in this below resonance region, the first order process involving the coupling of energy to half frequency spin waves is the limiting process in the high power operation of digital phase shifters.

The critical rf field strength at which first order high power effects set in can be expressed as:

$$h_{crit} = \frac{\omega_H \; \gamma^2 \; \Delta H \Delta H_k}{\gamma \omega_m \; \sin \theta_k \; \cos \theta_k \; (\omega_k + \omega_H - \omega_m \, N_Z + \omega_{ex} \ell^2 k^2)} \qquad (16)$$

where

ω_k	=	spin wave frequency
k	=	$2\pi/\lambda_k$ = spin wave number
λ_k	=	distance between spins that are in phase with one another
ω_H	=	γH where H is the applied field
ω_m	=	$\gamma 4\pi M_s$
N_Z	=	demagnetizing factor parallel to the dc field
ω_{ex}	=	γH_{ex}
H_{ex}	=	internal exchange field ($H_{ex} \sim 10^6$ gauss)
θ_k	=	angle between dc applied field and direction of $\vec{k}$
ℓ	=	lattice constant of material
ΔH	=	conventional uniform precessional linewidth
ΔH_k	=	"spin wave linewidth"

Thus by increasing the spin wave linewidth, ΔH_k, the power handling capability can be improved. However, a more effective and direct method can be used to increase high power handling ability. Figure 3 shows the usual spin wave manifold with the operating frequency ω and the first order spin wave frequency $\omega_k = \omega/2$ shown on the ordinate When sufficiently high rf power is applied $\left(h_{rf} > h_{crit}\right)$, energy at the signal frequency ω will be absorbed through conversion to the spin wave frequency $\omega_k = \omega/2$. If, however, the external field is raised so that the bottom of the spin wave manifold ω_b is
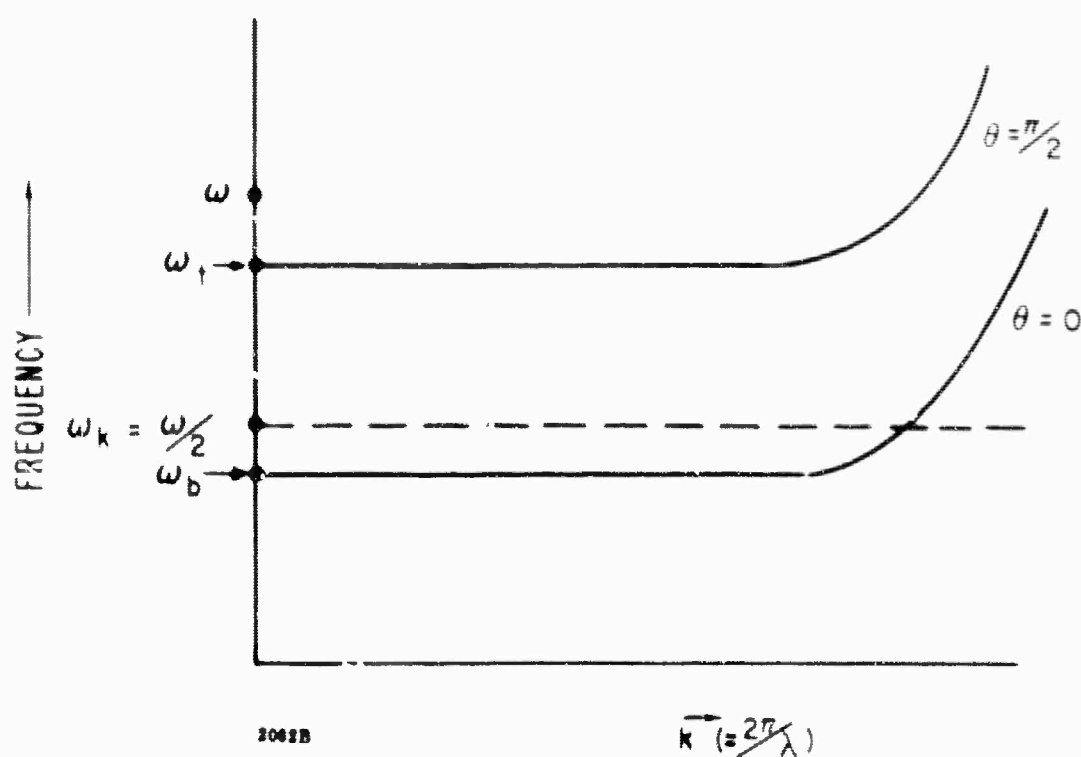
Figure 3. Operating Conditions for $\omega/2$ Spin Waves Within the Spin Wave Manifold

greater than $\omega/2$, then no spin waves will exist at $\omega_k = \omega/2$ and the first order process will be forbidden. This situation is depicted in Figure 4 and the threshold power level for subsidiary absorption will be extremely high.

Consider now the case shown in Figure 5, the normal set of conditions for very low applied fields. Here once again the spin wave frequencies $\omega_k = \omega/2$ are outside the spin wave manifold for low k, but at high k numbers, spin waves are degenerate with this frequency, This situation is not as favorable as that of Figure 4 when the first order process is forbidden, but does possess a higher threshold power level than the conditions of Figure 3. The higher threshold of Figure 5 arises from the fact that the spin wave linewidth varies with k as

$$\Delta H_k = A + Bk^2, \tag{17}$$

and by removing the degeneracy of the low k spin waves, scattering is forced to high k ($k \geq 10^5$) spin waves with larger spin wave linewidths and hence larger threshold power levels.

3-15
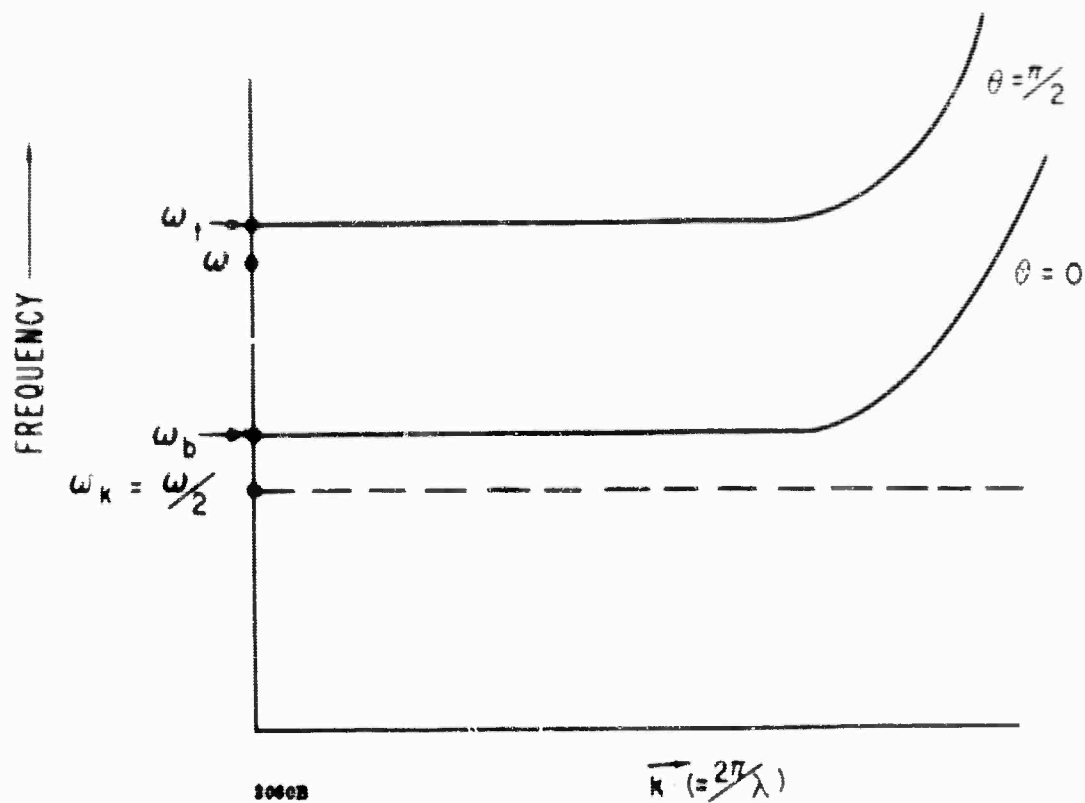
Figure 4. Operating Conditions for $\omega/2$ Spin Waves Below the Spin Wave Manifold
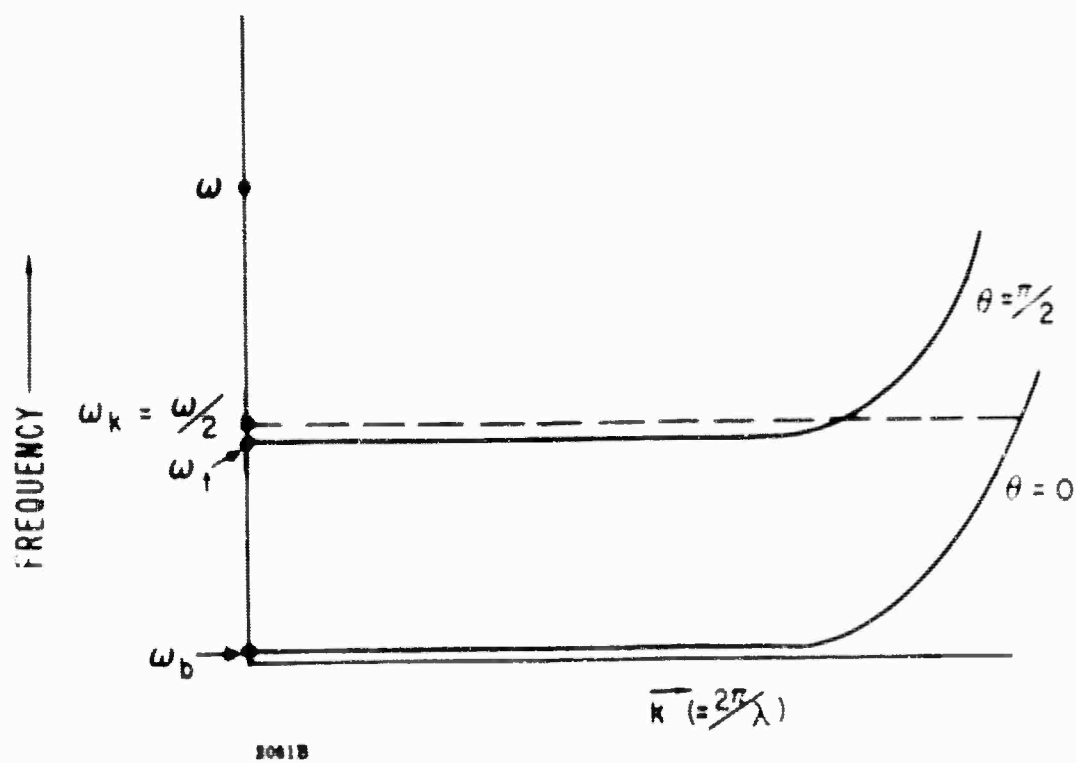
Figure 5. Operating Conditions for $\omega/2$ Spin Waves Above the Spin Wave Manifold

3-16

Since there is no field applied in latching phase shifters, the spin wave mani-
fold cannot be positioned with respect to the frequency axis by the action of an external
applied dc magnetic field. Instead, the positioning is controlled through selection of
the saturation magnetization with respect to the operating frequency.

To attain the condition of Figure 4 it is required that

$$\omega/2 < \omega_b = \gamma(H - N_Z 4\pi M) \tag{18}$$

If the magnetized vertical slab configuration as shown in Figure 6
(with $N_Z \approx 0.1$) is considered and if it is assumed that for a latching device $H \approx 4\pi M$,
then

$$\omega/2 < \omega_b = \gamma[4\pi M - (0.1)4\pi M]$$

$$\text{or} \quad \omega < 1.8\gamma 4\pi M \tag{19}$$

While this would be an extremely good condition for high power handling ability, it
would also correspond to operating latching phase shifters near or above resonance
and result in relatively small amounts of differential phase shifter per unit loss or
per unit length, respectively. Either situation is not desirable.

FERRIMAGNETIC
MATERIAL—

3066B
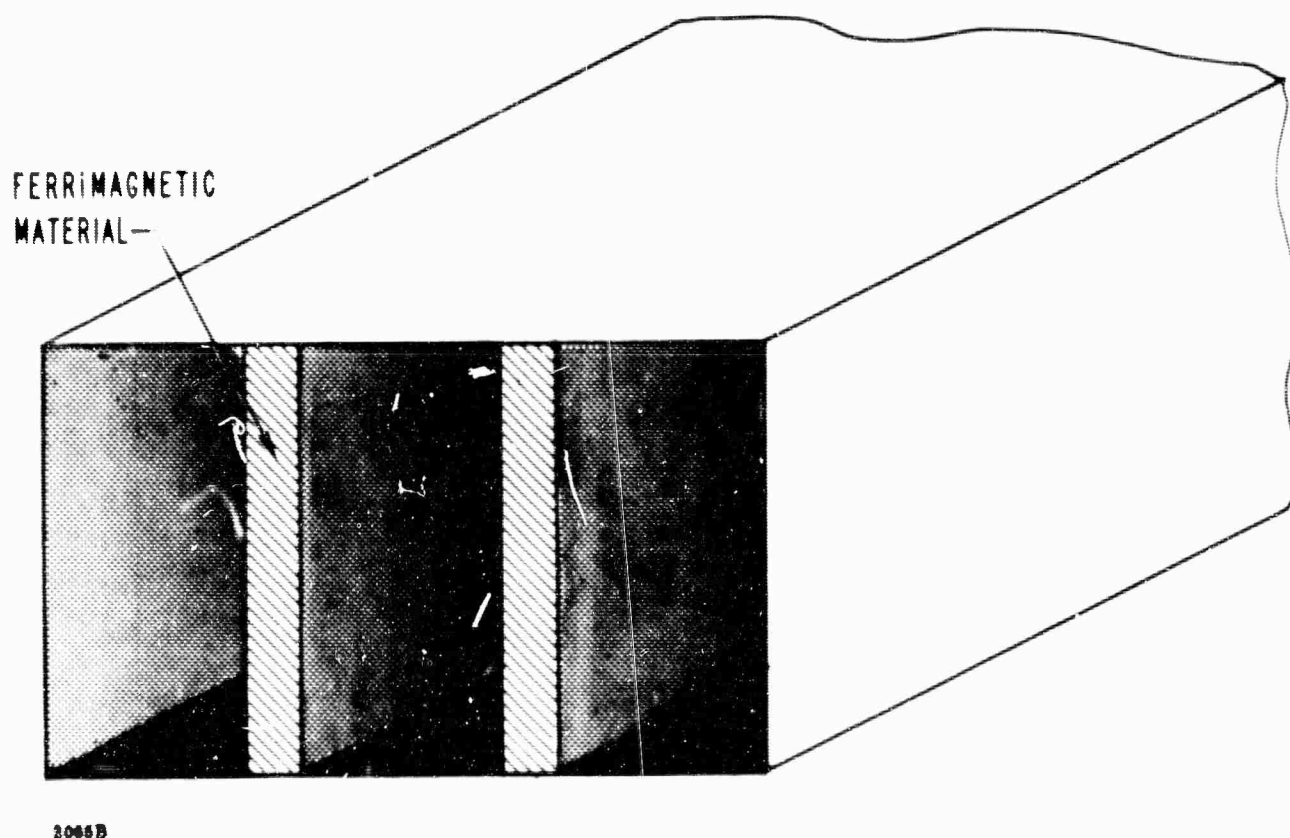
Figure 6. Vertical Slab Ferrite Geometry

To operate in the region shown by Figure 5 it is required that

$$\frac{\omega}{2} > \omega_t = \gamma \left\{ \left[H - N_z 4\pi M \right] \left[H + (1-N_z) \, 4\pi M \right] \right\}^{1/2}$$

Again taking $H \approx 4\pi M$, $N_z = 0.1$, the following result is obtained:

$$\frac{\omega}{2} > \gamma \left[(.9 \ 4\pi M) (1.9 \ 4\pi M) \right]^{1/2} \text{ or approximately} \qquad (20)$$

$$\frac{\omega}{2} > \gamma 1.3 (4\pi M). \qquad (21)$$

Thus the stability condition resolves to

$$\frac{\omega_m}{\omega} < .38 \qquad (22)$$

Thus for a given frequency ω, a value of saturation magnetization can be chosen such that the low k spin waves with small spin wave linewidths are all below the critical frequency $\omega/2$, and only those spin waves of high k and high spin wave linewidths, ΔH_k, will be coupled by first order effects to the uniform precession. This is a much more desirable region in which to operate from a low power standpoint since it corresponds to operation far below resonance, and therefore produces greater phase shift per unit loss and length than would materials fulfilling the requirements of Equation 19.

Shown in Figure 7 is a curve of critical field strength as a function of frequency for subsidiary resonance absorption on a sphere [9]. The data taken on a sphere show the effects of operating under the different condition of Figures 3, 4, and 5. The condition as per Figure 3 corresponds to the central region of this curve. The conditions of Figure 4 are reached at the upper end of this curve ($f \geq 3220$ mHz) when $\theta_k = 0$ and there are no longer spin waves of frequency $\omega/2$. The conditions of Figure 5 are reached at the lower end of this curve, near $f = 1765$ mHz, and scattering in this region is to spin waves with high k and large ΔH_k. Thus for high power handling ability either the operating conditions of Figure 4 or 5 may be employed. The dashed line of the upper curve of Figure 7 is a calculated curve assuming that ΔH_k is independent of k. The effects of its variation with k in accordance with equation (17) is clearly shown by the experimental points.

[9] E.G. Spencer, R.C. LeCraw and C.S. Porter, J Appl. Phys. 29, 429, (1958)
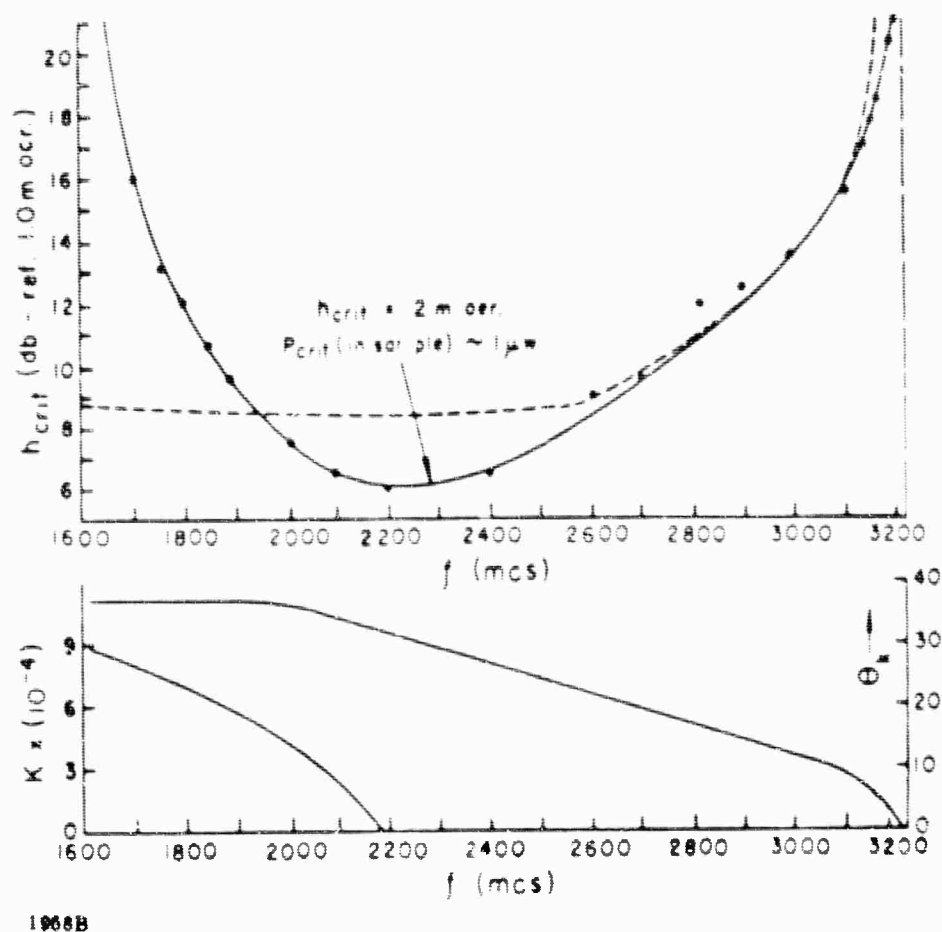
Figure 7. Calculated Values of h_{crit} Dashed Line of Upper Curves, k and θ (Lower Curves) as Functions of Frequency for Sphere of YIG. Curve Calculated Assuming ΔH_k is Constant. Measured Values of h_{crit} are the Solid Line of Upper Curve and Show the Importance of the Variation of ΔH_k with k.

Available experimental evidence on digital phase shifters shows a definite trend that agrees with the spin wave interpretation offered above. While the arguments are basically qualitative (particularly as regards to the assumption of $H \approx 4\pi M$), they supply a consistent and relatively clear insight into the physical phenomena involved. While the spin wave argument employed a manifold derived for cylindrical symmetry, the lack of such symmetry in phase shifter configurations will not disturb the basic precepts involved, but would probably slightly modify the numerical value of Equation 22. It is felt that the experimental points[6] of Figure 8 correspond to the lower portion of the curve of Figure 7 and the observed increase in h_{crit} is due principally to scattering to higher k number spin waves with large values of ΔH_k. It follows then that for best high power handling properties the lower the ratio of ω_m/ω the better, all else assumed equal.

[6] Ibid., p. 3-13
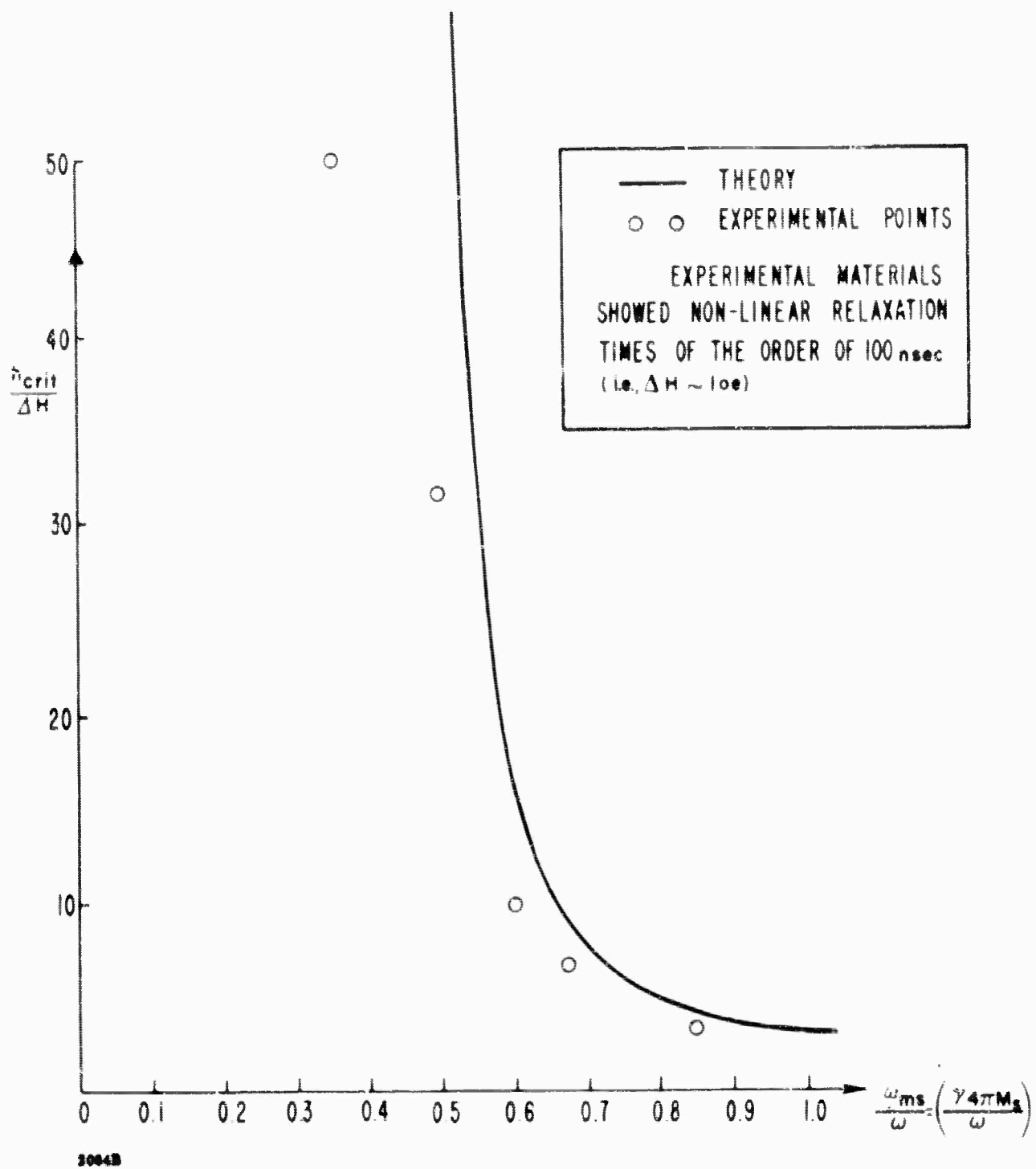
Figure 8. Critical RF Field Strength as Function of $(\gamma \cdots I_s)$ for Low Loss Ferrites and Garnets at L-and S-Band Freq encies (After H. Hair, footnote 6.)

The high power handling capability of a ferrite can also be increased by purposely doping the material with some ion having an intrinsicly high spin-lattice damping and a resultant large ΔH_k. Any such increase in ΔH_k of the material will increase the threshold power level as indicated in Equation 16. Much work has been carried out investigating this effect, and Figure 9 shows a summary of results obtained through rare earth doping of YIG. For example, as seen from these data, a 7 percent holmium doping of YIG increases the critical field by almost 40 fold to approximately 45 oersteds, equivalent to almost 500 kw peak power in X-band waveguide.

When rare earth doping is used to increase ΔH_k, and therefore the high power threshold, there is an accompanying increase in ΔH. On the other hand increasing ΔH_k by the previously described technique of restricting the scattering to high k spin waves is not accompanied by an increase in ΔH. Aside from this difference the two methods of achieving high threshold power levels are quite similar, and a combination of rare earth doping and control of saturation magnetization should make available materials with suitable power handling characteristics.

It has been shown that the use of extremely fine grained ferrites will result in very large threshold power levels. The device operation is generally as depicted in Figure 3 ($\frac{\omega}{2}$ spin waves are within the spin wave manifold), but spin wave coupling is strongest to those k numbers of the approximate dimensions of the grains; thus for fine grains, higher k values are the more strongly coupled and the peak power threshold increases. For the same compositions, larger grains would produce lower thresholds (coupling to lower k values). However, for the operating conditions of Figure 5 ($\frac{\omega}{2}$ above the spin wave manifold) the long wavelength spin waves to which large grains would tend to couple energy do not exist at $\omega_k = \frac{\omega}{2}$, and first order coupling to them is therefore forbidden. Under these operating conditions first order coupling is restricted to high k spin waves, and fine grain samples in this mode of operation would possibly result in lower peak power thresholds. For large grains the coupling mechanisms to high k values are small and the presence of fine grains would probably enhance these coupling mechanisms.

In addition to the above arguments, fine grain materials have exhibited high off-resonance electric and magnetic loss at low power levels. While the high electric loss can probably be reduced through processing improvement, the magnetic loss at low power seems associated with the particle size. It has been suggested that the use of fine grains enhances off-resonance loss at low power because the very short discontinuities give enhanced coupling to spin waves.
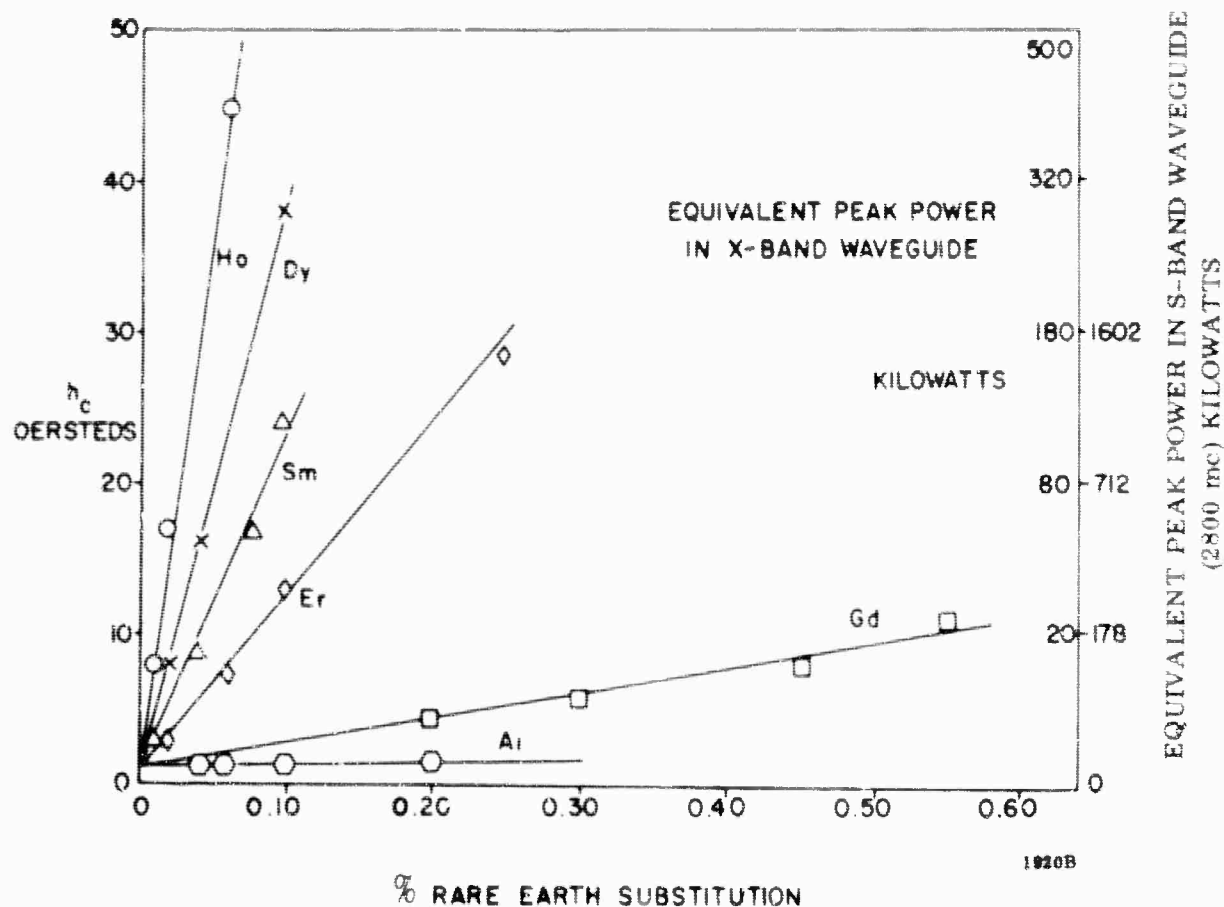
Figure 9. Critical Rf Field as a Function of Per Cent Rare Earth Substitution

Energy is coupled strongly to k values shorter than the discontinuities of the material. Phase shifter performance is very sensitive to such loss, and the additional loss of the fine grained material is highly undesirable. Moreover, our results have clearly demonstrated that best remanence ratios are obtained with the large grained materials. Therefore, it is felt preferable to employ large grains for good remanence values, and to achieve the desired power handling ability through control of ΔH_k by rare earth doping or through the control of the saturation magnetization and hence control of spin waves degenerate with $\frac{\omega}{2}$ or preferably a combination of these two techniques.

3.8 DESIRED MATERIAL CHARACTERISTICS

The following is a summary of the desired properties of ferrimagnetic materials for application in digital phase shifters.

1. Magnetization ($4\pi M_s$). Material should possess magnetizations suitable of application in phase shifters operating in the frequency region from L band through X band. Values from 100 gauss to approximately 2000 gauss are required. Temperature stability of the magnetization is desired where possible.

2. Remanence Ratio ($4\pi M_R / 4\pi M_s$). The remanence ratios should be the maximum obtainable. Values greater than 0.80 on all compositions are desired.

3. Ferromagnetic Linewidth (ΔH). Materials possessing low linewidths (less than 150 oersteds) are desired. The full importance of linewidth to the operation of FDPS is presently not established.

4. Dielectric Loss Tangent. Values less than 0.0001 (as measured at X band and room temperature) are desired.

5. Curie Temperature. Curie temperature values greater than 200° C are desired for all materials.

6. Dielectric Constant. Any value normally obtained in ferrimagnetic materials is acceptable provided reasonably good temperature stability and reproducibility is demonstrated.

7. Coercive Field (H_c). A value as low as possible consistent with the above properties is desirable. Values less than 1 oersted for all compositions are desired.

8. Anisotropy Field (H_{anis}). A value as low as possible for each material is desired.

9. Peak Power Threshold. For high power applications, the spin wave linewidth (ΔH_k) should be as large as possible consistent with the above desirable properties. The relationship
$$\frac{\gamma \, 4 \, \pi \, M_s}{\omega} < 0.4$$ should be maintained where possible.

10. Grain Size. Large average grain size is desired. The optimum value will depend on the composition. Values in the 10 to 30 micron area seem acceptable for most materials.

11. Density. Porosity and inclusions should be minimized; therefore maximum density should be maintained. Values of 97% or greater of theoretical density seem acceptable.

12. Stress and Strain. Unfavorable stresses and strains should be reduced to a minimum. Magnetostrictive energy should be minimum. At present, materials possessing magnetostrictive constants of zero or near zero appear to be most desirable.

13. Other properties. All other properties (g-factor, zero field permeability, etc.,) can be those which are compatible with the above properties.

14. Temperature Stability. As many properties as possible should exhibit temperature stability. The $4\pi M_S$ and $4\pi M_R$ values appear to be the most critical at the present.

BLANK PAGE

4. EXPERIMENTAL RESULTS

4.1 GENERAL

The program goals for this reporting period were as follows:

- Evaluate hysteresis properties of existing compounds
- Analytically interpret the desired material parameters
- Formulate new compositions
- Fabricate and evaluate these new compositions
- Establish optimized preparation procedure
- Design experimental rf test structures
- Initiate the evaluation of materials in rf structures

These goals have essentially been achieved in their entirety during this reporting period.

The following sections detail the experimental data and results obtained on the compositions investigated.

Before discussing the measured parameters, the apparatus employed to perform the magnetic and microwave measurements are discussed for completeness.

4.2 MAGNETIC AND MICROWAVE MEASUREMENT EQUIPMENT

Equipment is in operation for measuring the following properties of ferrimagnetic oxides: density, saturation magnetization, magnetic susceptibility as a function of magnetic biasing field, g-factor, linewidth, anisotropy field, Curie temperature, dielectric constant, dielectric loss tangents, remanence ratio, and coercive field. The equipment used to measure each of these properties, where appropriate can also be adapted for measurements as a function of temperature and frequency as well as rf power. The following equipment and techniques are being used for performing the measurements on this program. The equipment and techniques employed are in almost every case those specified by the ASTM Sub-Committee on Non-Metallic Magnetic Materials.

4.2.1 Measurement of $4\pi M_s$

The measurement of $4\pi M_s$ is made with the vibrating sample magnetometer shown in Figure 10. This measurement is based on the detection of the ac magnetic field set up by the vibrating magnetic sample. A small sphere of the unknown material
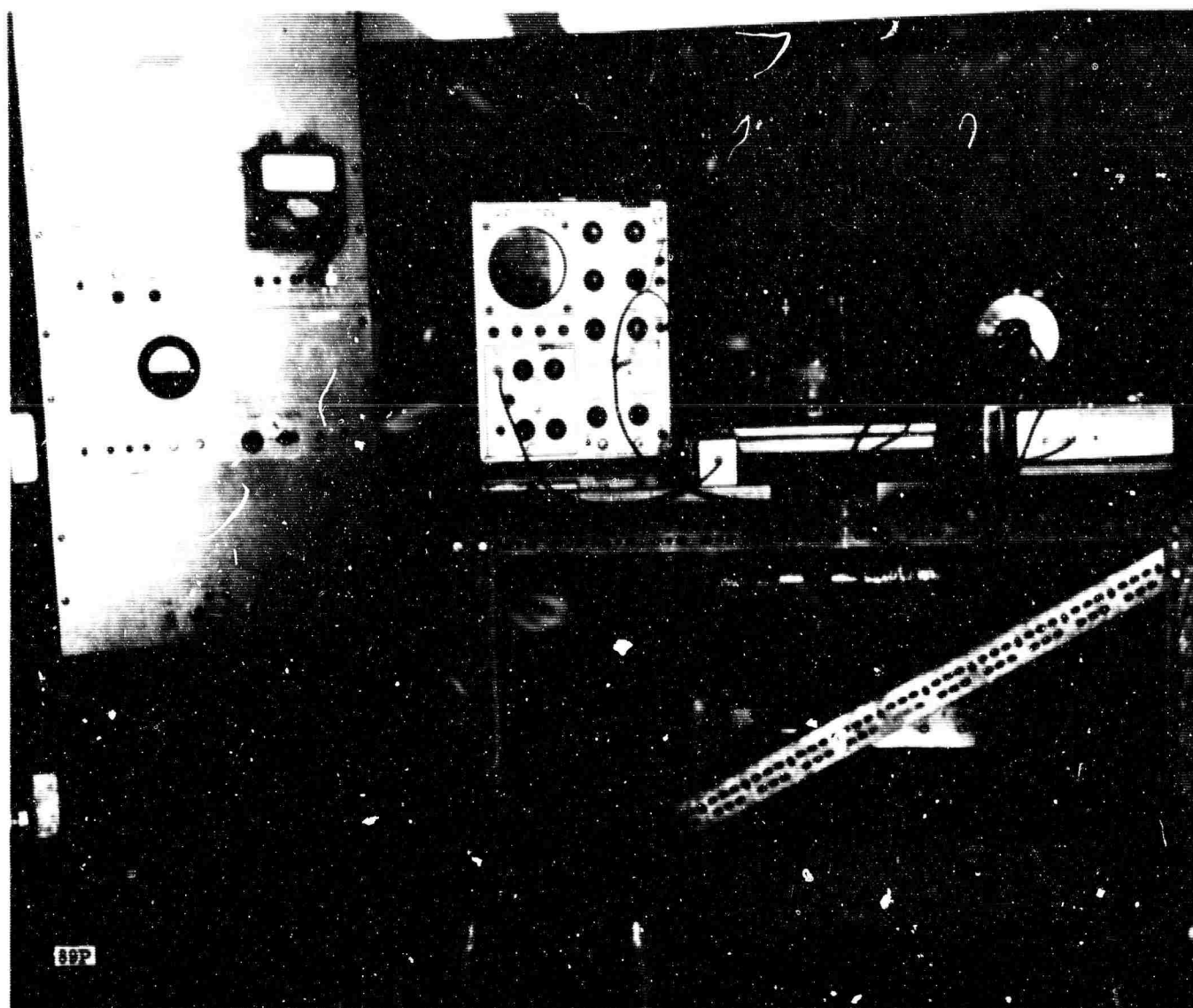
Figure 10.   Vibrating Sample Magnetometer

is placed in a strong saturating dc magnetic field.   The sample is vibrated at a low
audio frequency (100 cps) and the oscillating dipole field thus generated is detected by
two coils so positioned as to minimize stray pickup.   The magnitude of this dipole field
is compared to the signal detected by two similar coils from a known calibrated sample
attached to the same vibrating rod.   This system, first proposed by Foner,[10] is capable
of accurate, continuous readout and lends itself well to the measurement of saturation
magnetization as a function of temperature.   The magnetometer can also be used to
measure coercive force on spherical samples.

A new magnetometer is now nearing completion.   While it will be similar to
one discussed, it is expected to be more sensitive and more versatile with respect to
temperature measurements and readout procedures.   This magnetometer should be
operational in about two months.

---

[10] Foner, "Versatile and Sensitive Vibrating Sample Magnetometer," Rev. of Scientific
Instruments 30, 549 (1959)

4-2

4.2.2 Measurement of ΔH, g_{eff}-factor, Magnetic Susceptibility and Anisotropy Field

Reflection type resonance spectrometers are presently in use in this laboratory for V-, X-, and C-band measurements of linewidths. Coaxial equipment is now being set up for measurements at lower frequencies.

The samples measured are generally in the form of spheres 20 ±2 mils in diameter. The spheres are made by forcing a roughly cubical shaped sample of the material with compressed air around the inner periphery of a wheel which is coated with an abrasive powder. A 4/0 finish can easily be obtained using this method.

The effective g-factor is obtained simultaneously with the linewidth data by simply noting the field at which maximum absorption occurs and substituting this into Kittel's resonance equation. Figure 11 is a photograph of the X-band resonance spectrometer in Sperry's laboratory.
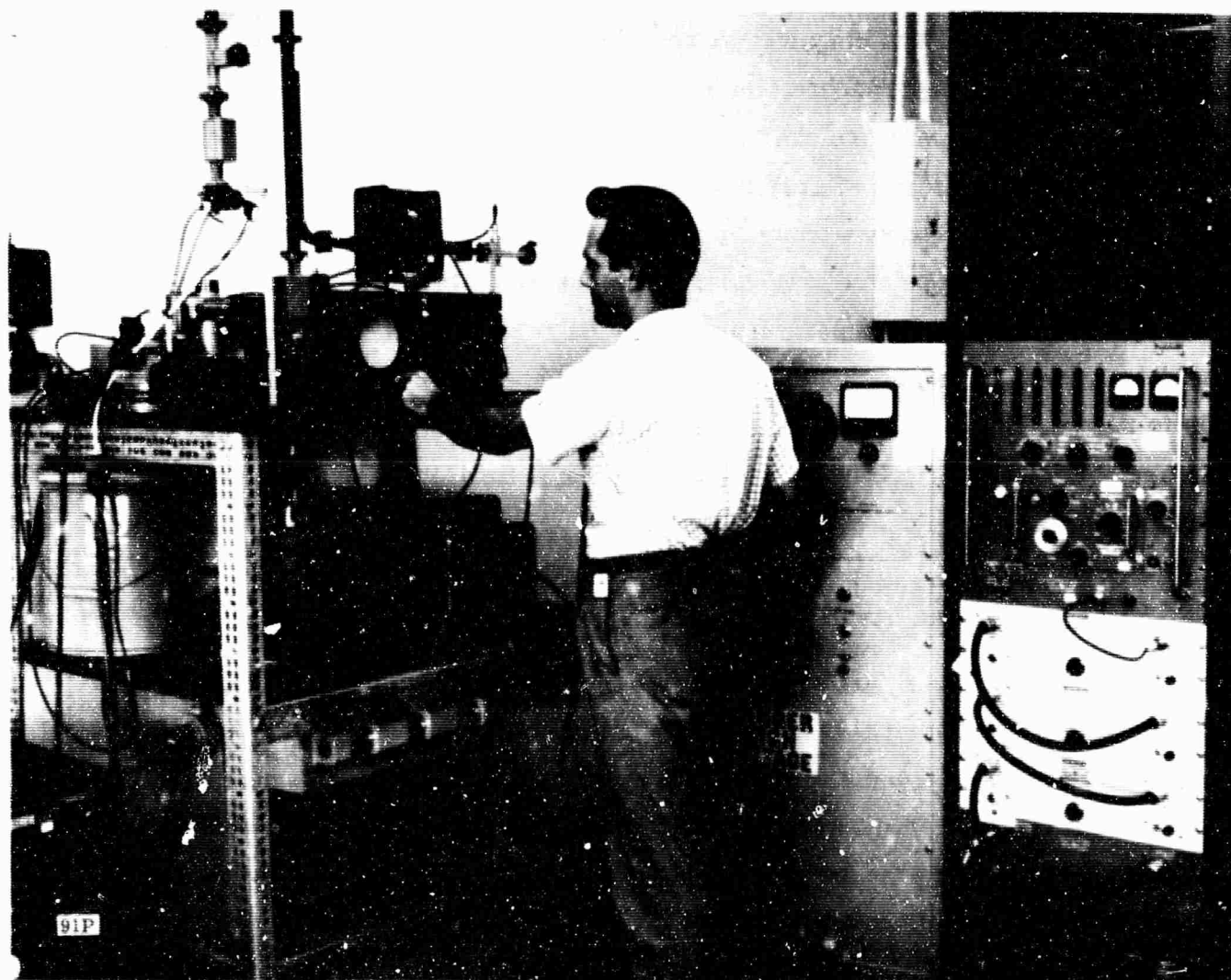
Figure 11. Reflection-Type Resonance Spectrometer, X Band

Single crystal linewidths are presently measured at C band. The techniques are well established for the simultaneous measurement of linewidth and $4\pi M_s$ for single crystal samples.

This same equipment can be used for the measurement of anisotropy field in aligned single crystal samples.

By monitoring the reflected signal from the cavity or shorted coaxial line as the field is varied, it is possible to obtain a plot of resonance line profile or imaginary part of the magnetic susceptibility as a function of applied field. Such plots are of considerable value when considering materials for off resonance applications such as phase shifters.

4.2.3 Measurement of T_c

Curie temperature measurements are done most rapidly with the simple furnace arrangement sketched in Figure 12. The test procedure is based on the balancing of gravitational and magnetic forces. As the temperature is raised and the Curie temperature is approached, the magnetization of a ferromagnetic body approaches zero. The Curie temperature can then be defined, in this measurement, as the temperature at which the force of gravity overcomes the magnetic force. The temperature at which the sample (S) drops from the magnet (P) can be determined by using two strips of foil (F) to close an electrical circuit and ring a bell when the sample forces the strips to touch. The temperature can then be read on a thermocouple. More precise determinations are made by measuring the temperature at which the magnetization falls to zero on the vibrating sample magnetometer of Figure 10. Curie temperature data are obtained directly when the saturation magnetization is measured as a function of temperature.

4.2.4 Measurement of Dielectric Constant (ϵ) and Dielectric Loss Tangent. ($\tan\delta$)

Measurements of dielectric loss tangent and dielectric constant are made at X band. A small cylindrical sample of the material to be measured is inserted in a transmission cavity at a point of maximum electric field and zero magnetic field. If the Q and the resonant frequency of the cavity are known before and after a sample is inserted, the $\tan\delta$ and ϵ can be calculated. $\tan\delta$ can be measured down to 0.0001 and ϵ values are accurate to about 5 per cent. Figure 13 is a photograph of this equipment.

4-4

THERMOMETER

INSULATION

C

P

S

F

BELL

18898
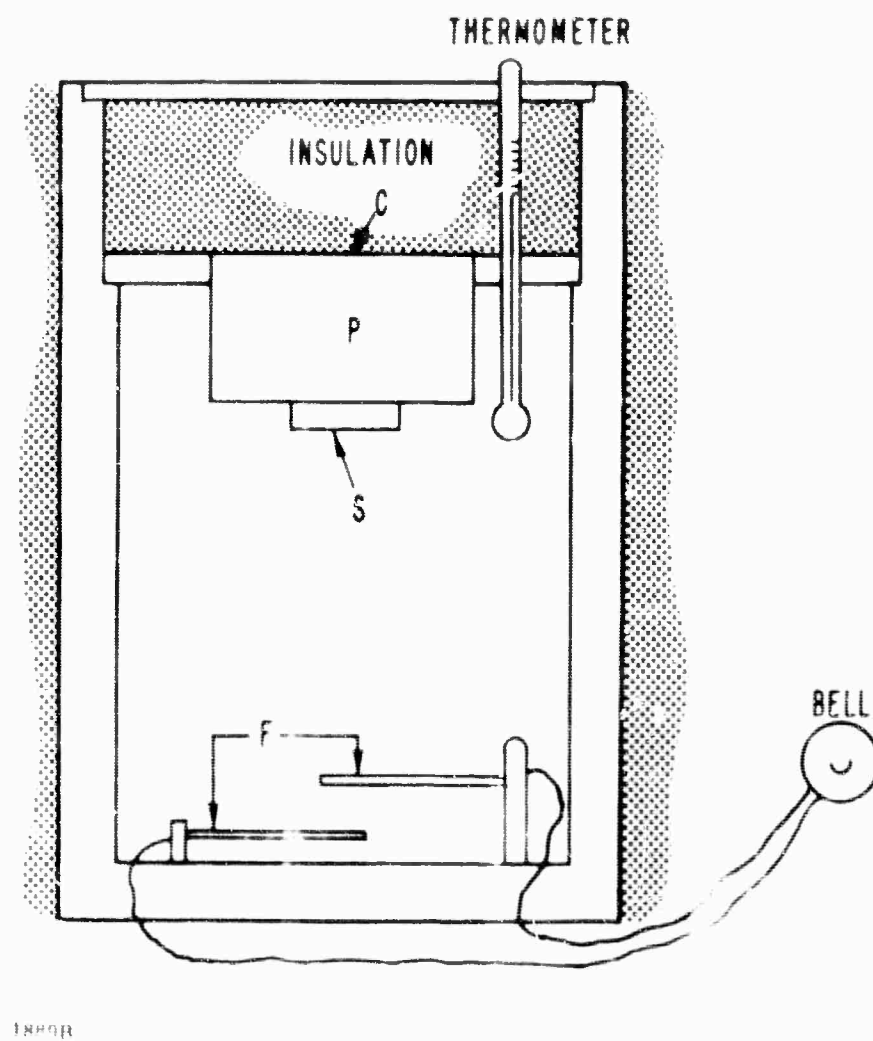
Figure 12. Furnace Arrangement for Simple Measurement of Curie Temperature. Explanatory Comments are in the Text.

1-5
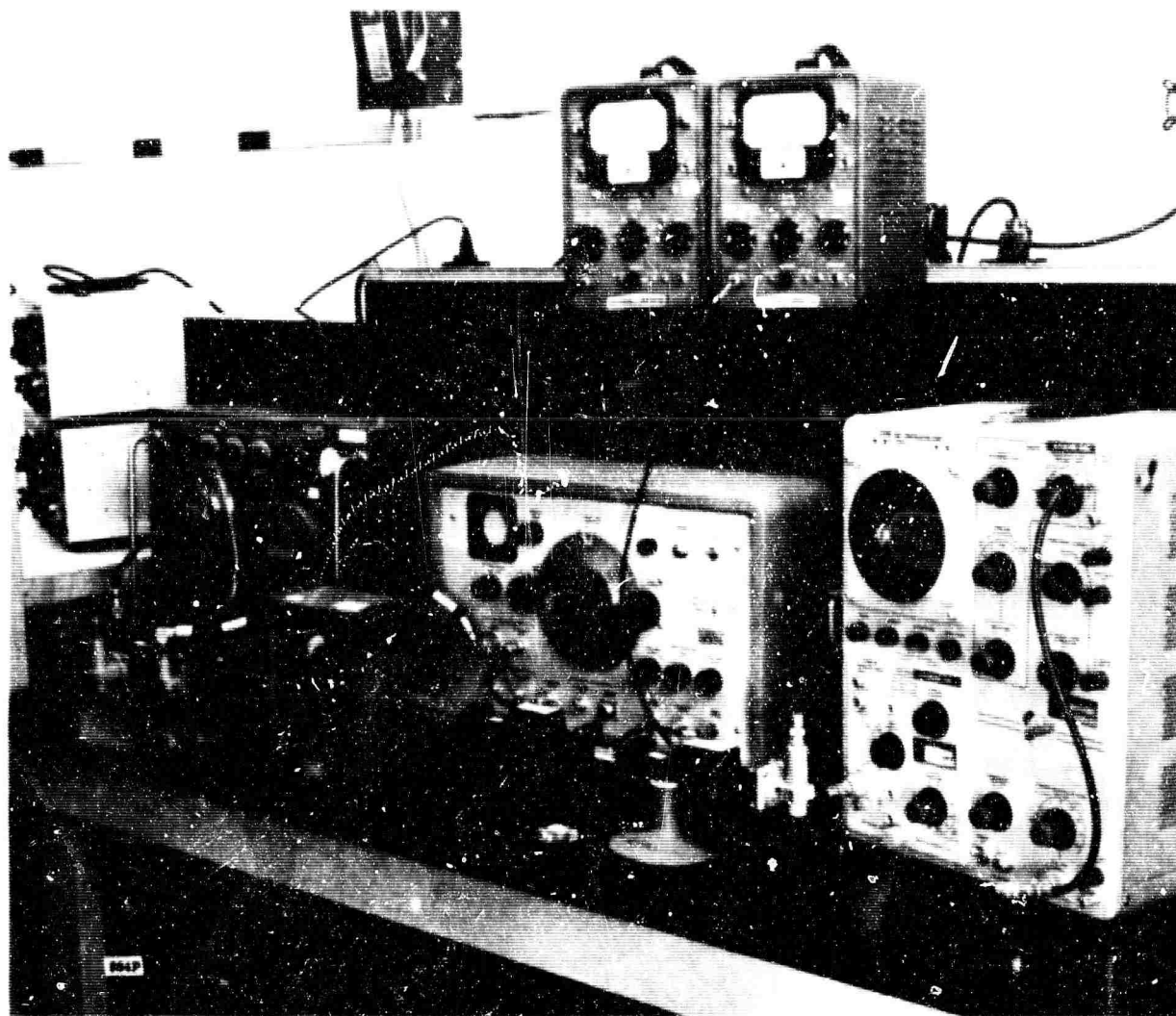
Figure 13. Dielectric Constant and Dielectric Loss Tangent Measurement
Equipment at X Band

Because of a growing need at Sperry for still more accurate determination of
low dielectric loss, a new cylindrical cavity is being constructed that permits an exact
solution for sample dielectric loss. A set of tables and charts will be completed to
facilitate the conversion of measured data to material parameters. This modified tech-
nique should greatly improve the accuracy of measurements of low dielectric loss
tangents.

4.2.5 Lattice Constants and X Ray Density

The lattice constants of various garnet and ferrite compounds will vary from
compound to compound. For a garnet of the series $5\,Fe_2O_3 \cdot 3\,(Y_{2-x}Gd_xO_3)$, if the
lattice constants of the end points (in this case YIG and GdIG) were known, the variation
of lattice constant with x can be calculated by Vergard's rule. The lattice constant of
these present materials can be determined from X ray diffraction data taken with the
X ray diffractometer of Figure 14 (Model G. E. XRD-5). The theoretical density of
the materials can be computed once the lattice constants and chemical composition are
known.

4-6
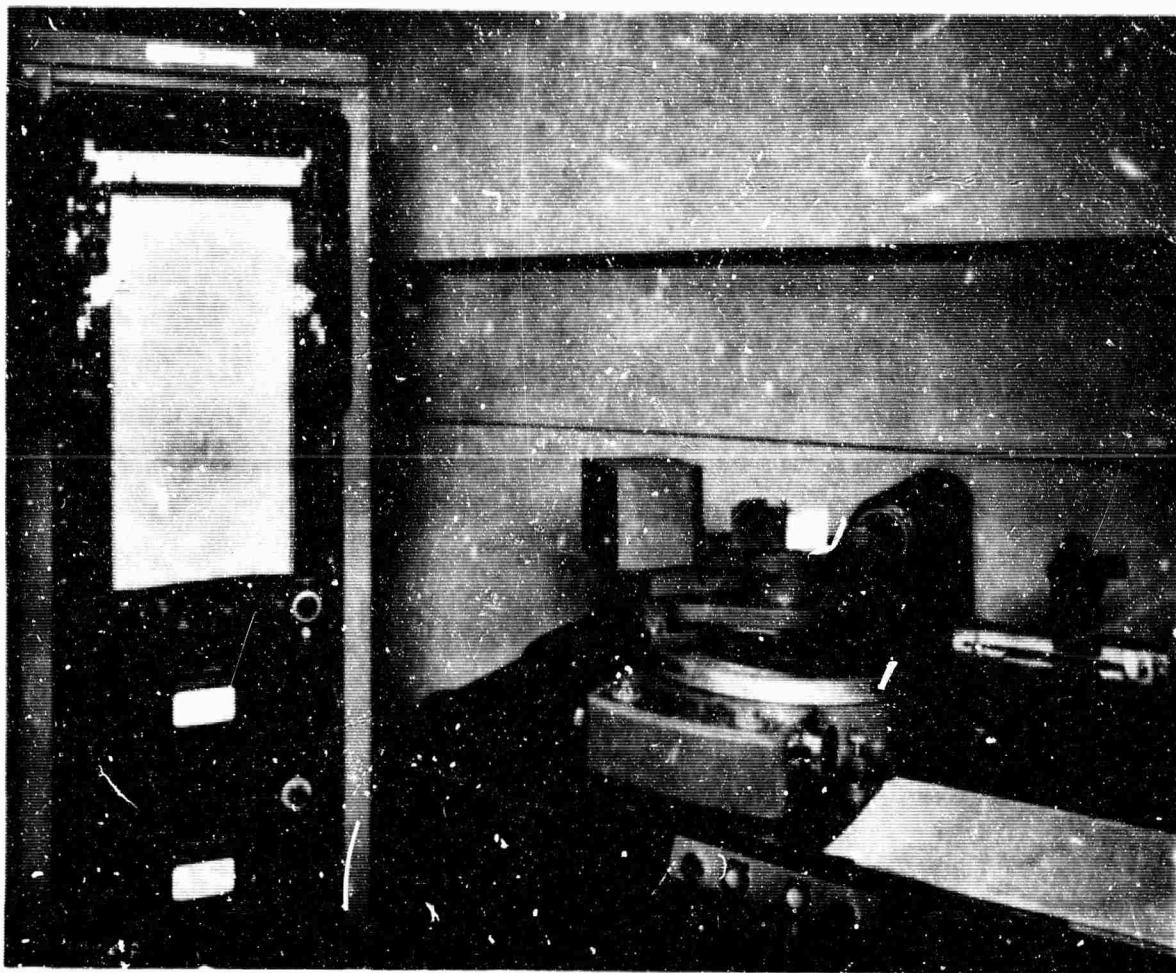
Figure 14.   General Electric XRD-5 X ray Diffractometer in Sperry
Microwave Electronics Company Laboratory

X ray diffraction data which is collected on this same apparatus can also be used to
study the phase purity of materials.

4.2.6 Measurement of Density

Density is measured in this laboratory by weighing accurately on chemical
balances, a sample of regular, measured dimensions, and by computing the ratio of
weight to volume.   For irregular samples, a mercury volumeter is used; this device
works by measurement of the buoyancy of the sample when immersed in mercury.

4.2.7 Measurement of Remanence Ratio and Coercive Field

A hysteresisograph or square loop tester has been built for the evaluation
and measurement of the hysteresis properties of ferrimagnetic oxides.   The equipment
operates at 60 cps and consists of a coaxial drive probe, integrator, function generator,
and scope display.   Remanence ratio and coercive field are read directly from digital
potentiometers.   A photograph of the square loop tester is depicted in Figure 15.

Figure 15.   Square Loop Tester

4. 2. 8 Particle Size and Shape

A Richert metallograph is available for use in the measurement of particle size and shape.   This instrument is capable of magnifications up to 2300 and is equipped with photographic attachments.   A photograph of the metallograph is shown in Figure 16.
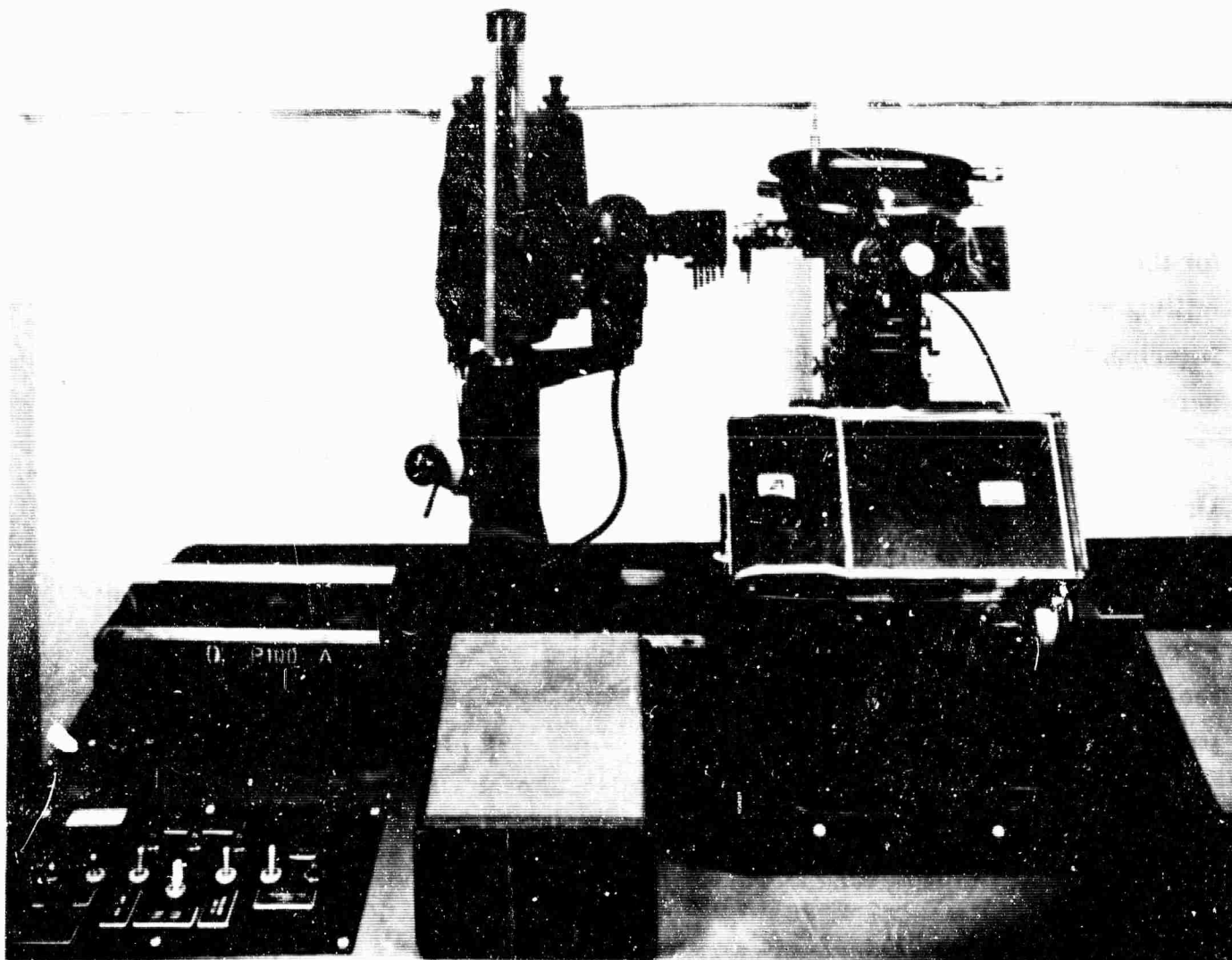
Figure 16.   Richert Metallograph Used for Material Evaluation

4.3 MATERIAL INVESTIGATIONS

The evaluation of existing compositions indicated that the garnet materials seemed to exhibit very desirable characteristics. The efforts therefore on new compositions have been primarily in the garnet family. Many different hybrid garnet compositions have been prepared and investigated. Special attention has been devoted to those compositions exhibiting temperature stability of the magnetization. These compositions are the gadolinum and aluminum substituted yttrium iron garnets.

Other rare earth (dysprosium, holmium, ytterbium, erbium, samarium) substituted yttrium iron garnets have been prepared and evaluated for possible high peak power applications.

4.3.1 Preparation Procedure

The square loop properties of these materials are strongly related to the process by which they are prepared. Therefore the preparation procedure has been given special attention during this reporting period.

4-9

A batch weight of 750 ± 5 grams was used for each composition. The oxides were mixed in stainless steel ball jars (1-3/4 gallons) containing 7500 grams of 1/2 inch diameter stainless steel balls. These conditions were established as standards for the initial materials preparation for this program. The oxides were mixed by ball milling with water for 8 hours. The water was removed from the solids by vacuum filtering. The oxides were dried at 110°C for 16 hours, screened through a 20 mesh screen, placed into a MgO boat and presintered at 1200°C for 8 hours.

The powder was ball milled with water after presintering to reduce the particle size, obtain a particle size distribution, and to introduce a binder (Mobilcer C, manufactured by Mobil Oil Company). The particle size in the final fired product may be changed by varying the ball milling time of this presintered material. The particle size of the powder continues to be reduced with increasing ball milling time. During the final firing operation, the increased rate of reaction resulting from the smaller particles causes increased grain growth in the final product. The limiting factor on ball milling time is iron pickup from the balls and mill. For the standard weight of material and ball mill size discussed above, excessive iron pickup occurs between 24 and 32 hours ball milling time as evidenced by an increased loss tangent at 32 hours.

After ball milling, the water is removed by vacuum filtering and the resulting solids dried at 80°C for 16 hours. The dried powder was then dry pressed into discs (1" O. D.) and toroids (0.485" O. D. x 0.275" I. D. x 0.5" long) using a pressure of 4 tons per square inch (tsi).

Firing was done in electric furnaces heated by silicon carbide elements. A continuous flow of oxygen was applied inside the firing zone to maintain oxidizing conditions and discourage the formation of divalent iron.

The sample nomenclature being used on this program is as follows:

Example: G-251 - 15   C

Designates a particular composition

Designates the batch number of this particular composition

Designates the particular sample pressed from this composition and batch

4-10
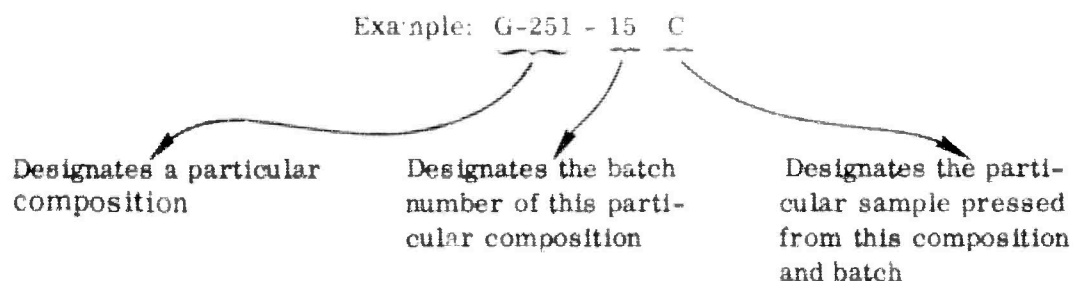
4.3.2 Particle Size Determination

The toroid sample which was used for measuring remanance ratio and coercive field was sliced in half with a diamond cutoff wheel. The newly exposed surface of the sample was then rough polished using 240, 320, 400 and 600 grit silicon carbide. The final polish was accomplished on a lapping wheel using diamond pastes of 6 and 1 micron particle size embedded in individual felt pads. After the proper polished surface was obtained, the sample was etched 5 minutes in a boiling solution of 50 cc water, 50 cc H_2SO_4 and 1 gram of oxalic acid to expose the grain boundaries.

Photomicrographs, 500 magnification, were taken of the etched surface of the sample using a Reichert metallograph. Transparent material printed with hexagonal shapes were prepared as overlays for the photomicrographs. The distance between parallel sides of the hexagonal shapes were made to correspond to 5, 7, 11, 13, 16, 20, 22, 25 and 29 microns at 500 magnification. The particle size of the sample was then determined by comparison of the overlays with the photomicrograph.

4.3.3 Measured Properties

The compositions and properties of the materials prepared and evaluated during this period are listed in Table I. The materials are all garnets and are listed in accordance with their measured value of magnetization ($4\pi M_s$), starting with a value of approximately 1800 gauss and decreasing to 100 gauss.

The following family of materials has been investigated:

$$3\left[(1-x)\ Y_2O_3 \cdot x\ RE_2O_3\right] \cdot 5\left[(1-w)\ Fe_{1.925}O_3 \cdot w\,T_{1.925}O_3\right]$$
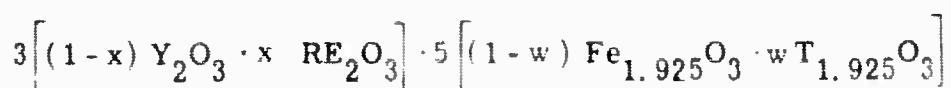
where

RE represents the rare earth oxides of gadolinium, dysprosuim, samarium, ytterbium, erbium and holmium, and

T represents the transition metal oxides of aluminum and gallium

The yttrium gadolinium iron and the yttrium gadolinium aluminum iron garnet families have been given special attention during this period principally because these materials possess magnetizations which are temperature independent. The temperature characteristics of many of these materials had been studied prior to the start of this program. Some of these data are presented in Figures 17, 18, 19, 20, 21, and 22 to illustrate the degree of temperature compensation and that materials possessing almost any value of magnetization ($4\pi M_s$) up to a value of approximately 1200 gauss can be

prepared and temperature compensated. The hysteresis properties of these materials have been measured and evaluated on this program as listed in Table I.

The rare earth substituted yttrium iron garnets have been investigated principally to evaluated their hysteresis and high peak power characteristics. These rare earth substitutions are known to improve peak power threshold (increase ΔH_k) for normal applications as illustrated in Figure 9.

Grain Size Measurements. Investigations indicate that grain size is very important in optimizing the hysteresis properties of ferrimagnetic materials. The grain size is principally controlled by the preparation procedure (ball milling time and firing temperature).

A variation in particle size was produced in samples of composition No. G-251-15 (15% gadolinium - 5% aluminum substituted yttrium iron garnet) by firing at 25°C intervals from 1375 to 1500°C. A sharp rise in remanence ratio, R_R, and a marked decrease in coercive field, H_c, were observed as the average particle size increased from 3 to 12 microns. These data are presented in Figure 23. The measured properties and preparation parameters of these compositions are presented in Table II. Photographs showing the increase in grain size are presented in Figure 24.

TABLE II

Measured Properties and Preparation Parameters

$$3(0.85 \; Y_2O_3 \cdot 0.15 \; Gd_2O_3) \cdot 5 \; (0.05 \; A\ell_{1.925}O_3 \cdot 0.95 \; Fe_{1.925}O_3)$$

G-251-15 [Waxing Time - 24 Hours]

Toroid No.	Density (gm/cm^3)	R_R	H_c (Oersteds)	Particle Size (Microns)	Firing Temp. Time $^{\circ}$C/Hr
G-251-15Y	4.99	0.62	2.71	3-4	1375/5
G-251-15W	5.10	0.71	2.25	4-5	1400/5
G-251-15S	5.30	0.78	1.53	6	1425/5
G-251-15V	5.27	0.80	0.94	11	1450/5
G-251-15T	5.33	0.86	0.86	12	1475/5
G-251-15R	5.26	0.89	0.61	19	1500/5
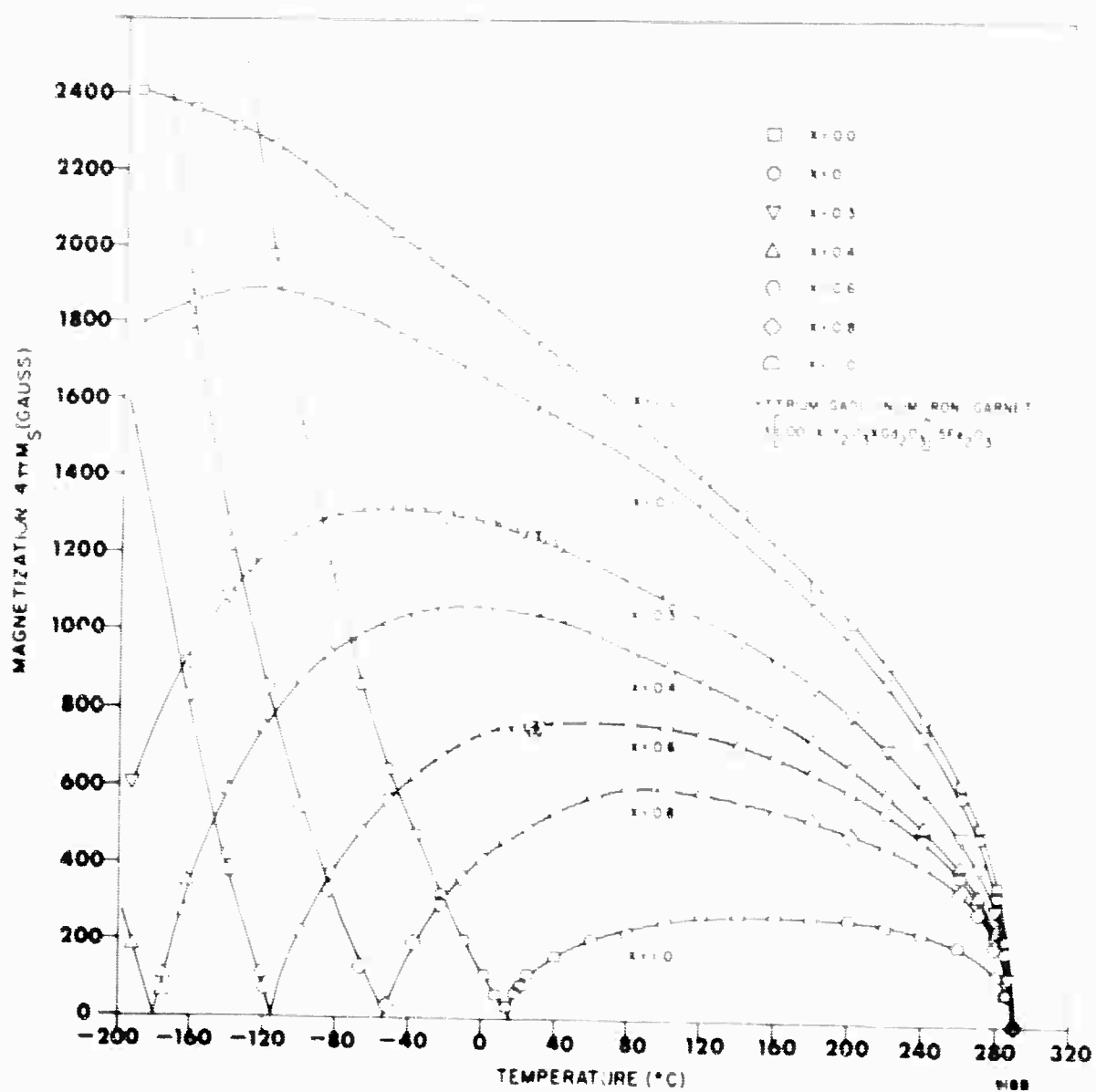
Figure 17. The Variation of Saturation Magnetization with Temperature for Yttrium Gadolinium Iron Garnet

Figure 18. The Variation of Saturation Magnetization with Temperature for Aluminum Substituted 85% YIG · 15% GdIG

4-14

Figure 19. The Variation of Saturation Magnetization with Temperature for Aluminum Substituted 80% YIG · 20% GdIG
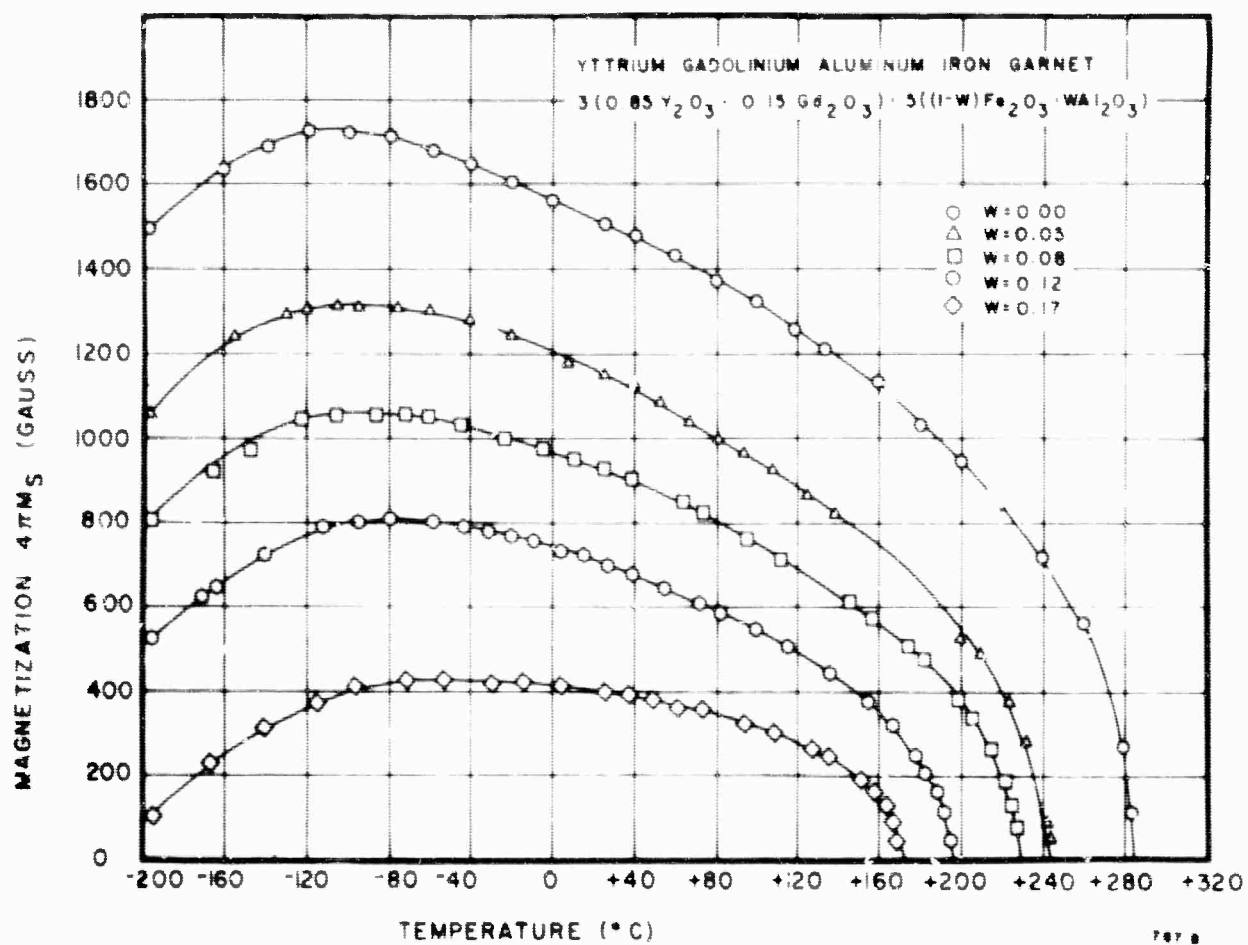

Figure 20. The Variation of Saturation Magnetization with Temperature for Aluminum Substituted 75% YIG · 25% GdIG
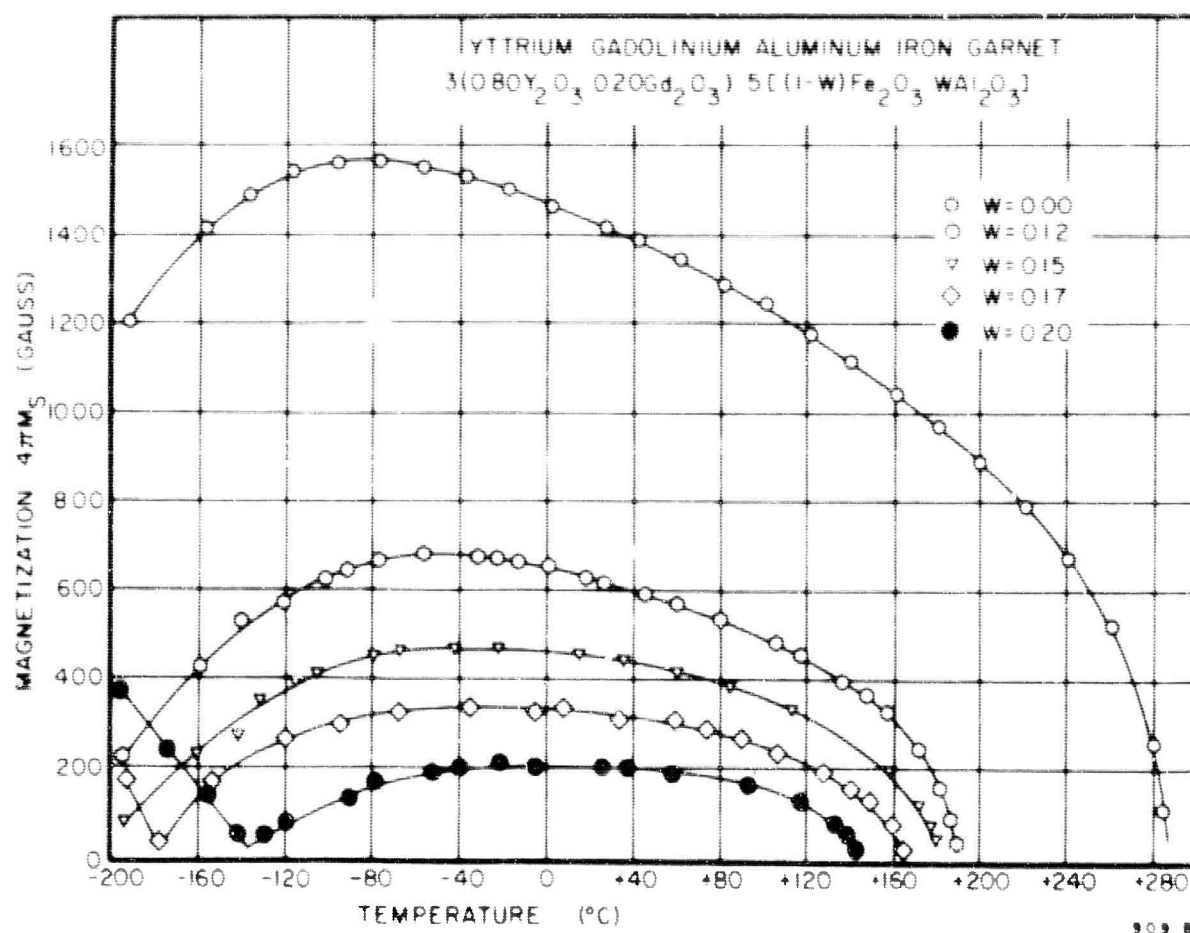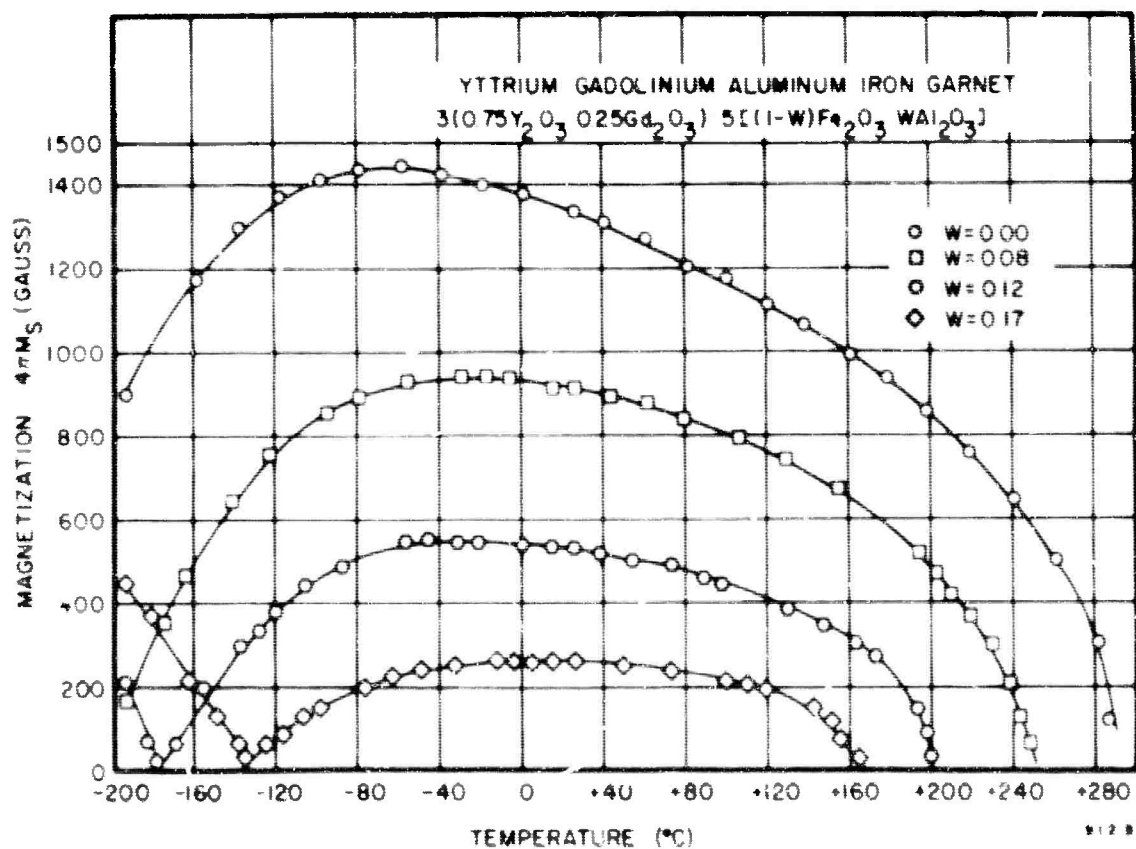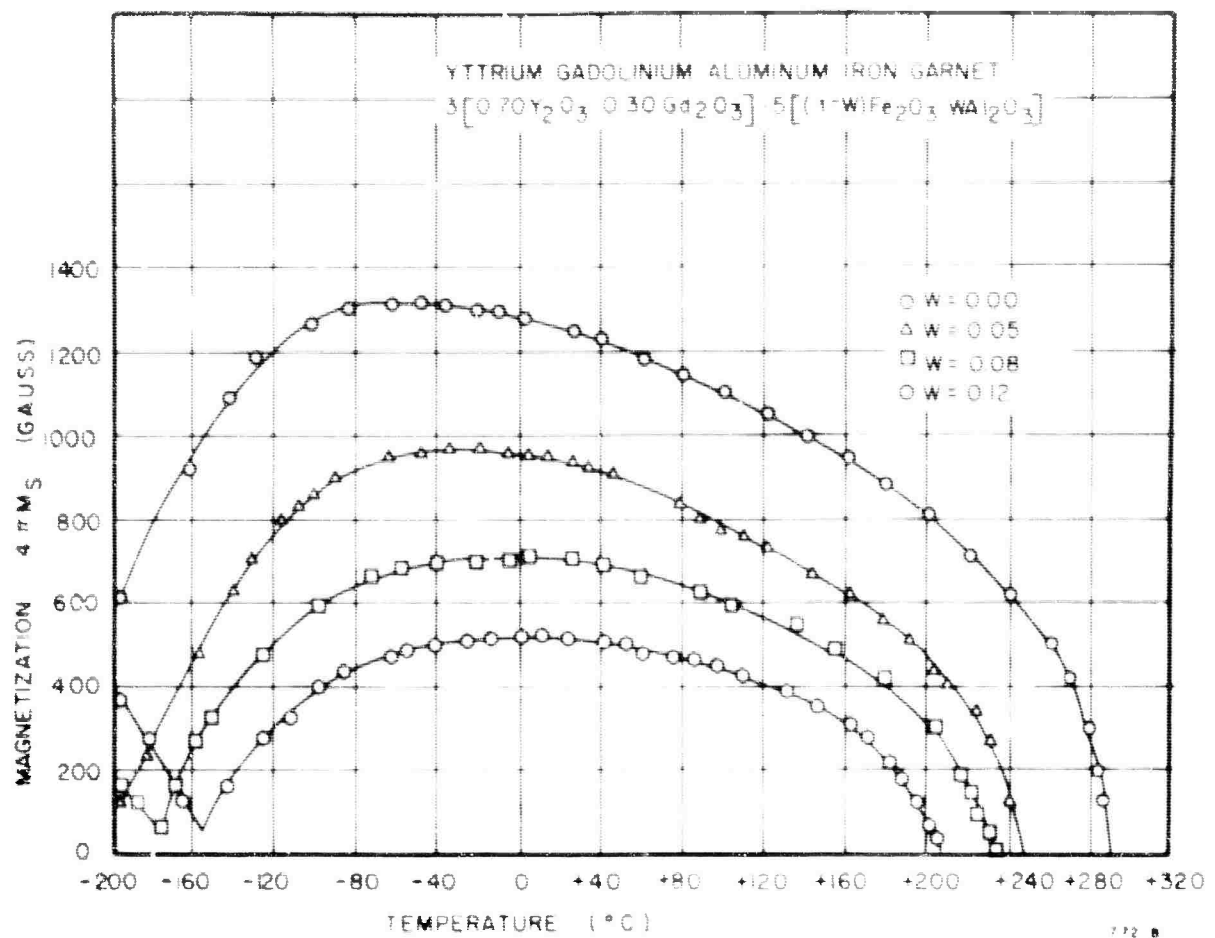
Figure 21. The Variation of Saturation Magnetization with Temperature for Aluminum Substituted 70% YIG · 30% GdIG
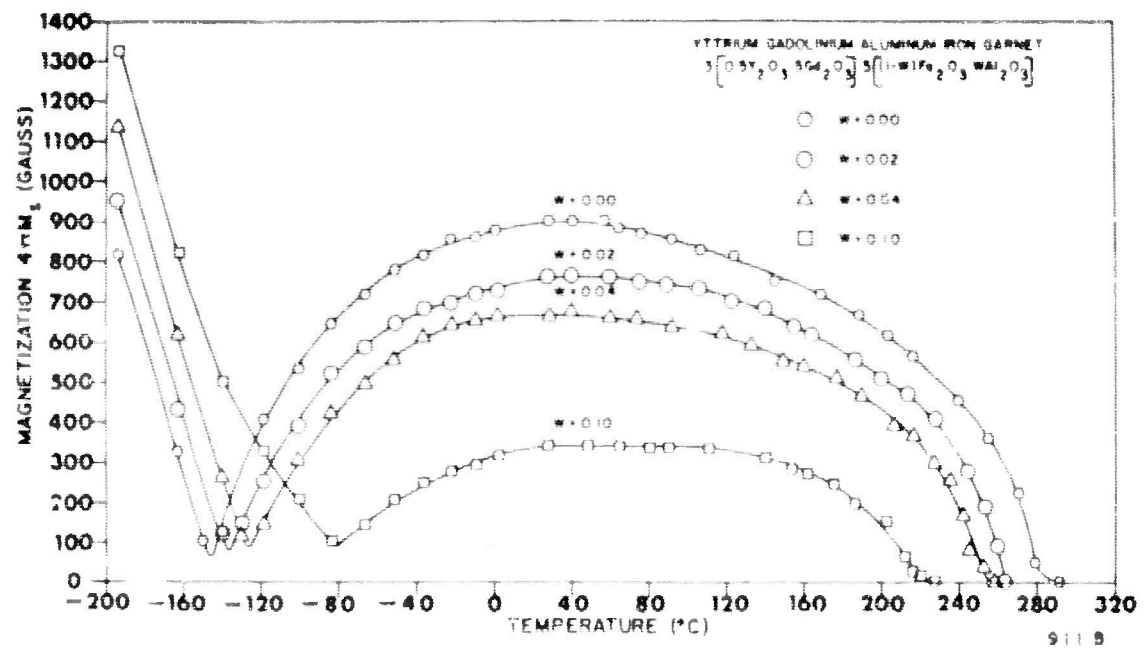

Figure 22. The Variation of Saturation Magnetization with Temperature for Aluminum Substituted 50% YIG · 50% GdIG

BLANK PAGE

Table I. Compositions Prepared and Evaluated

$$3\left[(1-x)\,Y_2O_3 \bullet x\,RE_2O_3\right] \bullet 5\left[(1-w)\,Fe_{1.925}O_3 \bullet w\,T_{1.925}O_3\right]$$

Start No.	Composition x	Composition w	Density gm/cm²	4πMs (gauss) 25°C	ΔH(oe) (at Band)(25°C)	g Factor	Remanence Ratio (Br) 60~, 25°C	Coercive Field (Hc) Oe 60~, 25°C	Drive Field (H₀)(oe)	Particle Size Microns	Firing Temp °C/Hr	Mixing Time Hrs	Loss Tangent X Band	Dielectric Constant (ε) X Band
G325A	0.10 Sm	-	5.20	1830	180	2.00	0.83	0.70	2.45	14	1475/5	24	.0037	16.2
G325C	0.10Sm	-	5.17	NM	NM	NM	0.79	0.66	2.99	16	1500/5	24	.0001	15.9
G323A	0.10Yb	-	5.28	1810	65	2.00	0.82	0.51	1.46	18	1475/5	24	.0064	16.2
G323C	0.10Yb	-	5.26	NM	NM	NM	0.73	0.56	1.79	18	1500/5	24	.0005	16.0
G322A	0.05Ho	-	5.18	1800	245	2.00	0.88	0.57	1.27	13	1475/5	24	.0001	15.9
G322C	0.05Ho	-	5.17	NM	NM	NM	0.88	0.41	1.18	21	1500/5	24	.0002	15.9
G289E	-	-	5.08	1800	36	2.01	0.89	0.44	1.19	16	1500/5	16	.0001	15.7
G289C	-	-	5.11	1780	33	2.02	0.90	0.47	1.38	16	1475/5	16	.0001	16.0
G345B	0.01Dy	-	5.10	1780	80	2.00	0.88	0.61	1.29	NM	1475/5	16	.0001	16.1
G130-2B	0.04Dy	-	5.12	1760	150	1.96	0.90	0.63	1.28	NM	1475/5	8	.0001	15.9
G307C	0.02Ho	-	5.09	1760	95	2.00	0.92	0.40	1.04	NM	1475/5	16	.0001	16.0
G324A	0.10Er	-	5.25	1755	110	1.96	0.87	0.53	1.48	16	1475/5	24	.0009	15.8
G324C	0.10Er	-	5.22	NM	NM	NM	0.86	0.47	1.66	19	1500/5	24	.0003	15.4
G75-2B	0.075Sm	-	5.12	1750	140	2.00	0.87	0.79	1.35	NM	1475/5	8	.0001	16.2
G121-2B	0.10Er	-	5.22	1745	130	1.96	0.89	0.60	1.33	NM	1475/5	8	.0001	16.1
G321A	0.08Dy	-	5.23	1720	230	1.90	0.87	0.60	1.25	12	1475/5	24	.0002	16.1
G321C	0.08Dy	-	5.18	NM	NM	NM	0.87	0.44	1.34	21	1500/5	24	.0001	16.0
G196-2B	0.15Er	.	5.30	1700	160	1.92	0.89	0.62	1.29	NM	1475/5	8	.0001	16.1
G197-2B	0.25Er	-	5.50	1600	260	1.86	0.87	0.67	1.82	NM	1475/5	8	.0007	15.9
G290E	-	0.03Al	5.08	1600	34	2.01	0.90	0.41	1.00	NM	1500/5	16	.0002	15.7
G290C	-	0.03Al	5.11	1590	25	2.01	0.90	0.57	1.57	16	1475/5	16	NM	NM
G295C	0.15Gd	-	5.32	1530	37	2.02	0.87	0.65	1.62	13	1475/5	16	NM	NM
G301E	0.15Gd	0.02Al	5.28	1425	53	2.02	0.83	0.43	1.03	NM	1500/5	16	.0001	15.7
G326A	-	0.05Ga	5.17	1420	25	2.01	0.88	0.66	1.40	10	1475/5	16	.0001	15.8
G326C	-	0.05Ga	5.17	NM	NM	NM	0.88	0.49	1.45	14	1500/5	16	.0001	15.7
G301C	0.15Gd	0.02Al	5.30	1365	4.	2.01	0.98	0.68	1.97	13	1475/5	16	NM	NM

RE = Rare Earths
Y = Yttrium
Gd = Gadolinium
Dy = Dysprosium
Yb = Ytterbium
Er = Erbium
Ho = Holmium
T = Transition Metal
Al = Aluminum
Ga = Gallium
NM = Not measured to date

Table I. Compositions Prepared and Evaluated (continued)

$$3\left[(1-x)\,Y_2O_3 \cdot x\,RE_2O_3\right] \cdot 5\left[(1-w)\,Fe_{1.925}O_3 \cdot w\,T_{1.925}O_3\right]$$

Samp No	Composition x	Composition w	Density gm/cm²	4πMs (gauss) 25°C	ΔHk (X Band)(25°C)	Spin Factor	Remanence Ratio 60°, 25°C	Coercive Field (Hci) 60°, 25°C	Drive Field (Hd)(oe)	Particle Size Microns	Firing Temp °C/hr	Wetting Time Hrs	Loss Tangent X Band	Dielectric Constant(ε) X Band
G296C	0.30Gd		5.31	1270	43	2.02	0.71	1.01	1.88	14	1475/5	16	NM	NM
G296-3C	0.30Gd		5.52	1260	71	2.02	0.65	1.22	3.09	12	1475/5	8	.0001	16.2
G296-2C	0.30Gd		5.45	1240	82	2.02	0.90	0.68	1.79	22	1475/5	24	.0001	15.8
G-296-6C	0.30Gd		5.51	1240	80	2.02	.84	.77	1.70	NM	1475/5	32	.0036	16.3
G299C	0.30Gd 0.02Dy		5.54	1240	127	1.98	0.78	1.02	2.10	NM	1475/5	16	NM	NM
G300C	0.30Gd 0.04Dy		5.56	1220	170	1.94	0.87	1.01	2.64	NM	1475/5	16	NM	NM
G291E		0.08Al	5.06	1195	32	2.01	0.90	0.47	1.39	11	1500/5	16	.0001	15.5
G251-9U	0.15Gd	0.05Al	5.22	1170	54	2.02	0.88	0.82	1.91	18	1500/5	16	.0001	15.6
G284C	0.01Ho	0.08Al	5.10	1165	72	2.00	0.90	0.74	1.72	8	1475/5	16	.0001	NM
G285C	0.03Ho	0.08Al	5.14	1155	153	1.97	0.90	0.77	1.71	8	1475/5	16	.0001	15.5
G291C		0.08Al	5.10	1150	24	2.01	0.90	0.65	1.58	8	1475/5	16	NM	NM
G288C	0.15Gd 0.02Dy	0.05Al	5.34	1135	104	1.98	0.80	1.10	2.97	12	1475/5	16	NM	NM
G251-9C	0.15Gd	0.05Al	5.24	1130	52	2.02	0.87	0.90	2.00	13	1475/5	16	.0001	15.6
G287C	0.04Dy	0.08Al	5.15	1120	138	1.94	0.89	0.81	1.84	8	1475/5	16	NM	NM
G286C	0.02Dy	0.08Al	5.12	1115	80	1.97	0.90	0.72	1.38	8	1475/5	16	.0001	15.5
G297-2A	0.45Gd		5.68	1100	105	2.03	0.77	1.57	4.22	11	1475/5	24	NM	NM
G341B	0.40Gd 0.02Dy		NM	1090	NM	NM	0.87	0.95	2.69	NM	1475/5	24	.0001	16.2
G297-2C	0.45Gd		5.65	1075	112	2.03	0.76	1.09	2.62	18	1500/5	24	.0001	16.2
G297C	0.45Gd		5.70	1040	10	2.03	0.66	1.40	3.57	16	1475/5	16	NM	NM
G327A		0.10Ga	5.18	985	27	2.01	0.89	0.68	1.81	9	1475/5	16	.0001	15.7
G327C		0.10Ga	5.19	NM	NM	NM	0.88	0.50	1.95	14	1500/5	16	.0001	15.6
G305B	0.15Gd	0.07Al	5.18	950	70	2.02	0.85	0.80	2.22	NM	1475/5	8	NM	NM
G333A	0.50Gd		5.78	940	135	2.03	0.78	1.17	2.99	16	1475/5	24	.0001	16.4
G333C	0.50Gd		5.77	NM	NM	NM	0.76	1.09	2.92	19	1500/5	24	.0001	16.4
G330A	0.30Gd	0.05Al	5.49	935	75	2.02	0.86	1.02	2.51	14	1475/5	24	.0001	16.0
G330C	0.30Gd	0.05Al	5.43	NM	NM	NM	0.86	0.67	1.60	22	1500/5	24	.0001	15.8
G328A	0.30Gd	0.65Ga	5.53	900	85	2.02	0.85	1.04	2.45	12	1475/5	24	.0001	15.9

4-18

Table I. Compositions Prepared and Evaluated (continued)

$$3 \left[(1-x) Y_2O_3 \cdot x RE_2O_3\right] \cdot 5 \left[(1-w) Fe_{1.925}O_3 \cdot w T_{1.925}O_3\right]$$

SMC No.	Composition x	Composition w	Density gm/cm²	4πMs (gauss) 7.5°C	ΔH(oe) (X Band)(25°C)	Het Factor	Remanence Ratio (Br/Bm) 60~, 25°C	Coercive Field Hc (oe) 60~, 25°C	Drive Field (Hd)(oe)	Particle Size Microns	Firing Temp °C/hr	Washing Time Hrs	Loss Tangent x Band	Dielectric Constant(e') x Band
G328C	0.30Gd	0.05Ga	5.51	NM	NM	NM	0.87	0.72	1.85	25	1500/5	24	.0001	15.7
G292C		0.12Al	5.07	890	25	2.01	0.90	0.83	1.88	6	1475/5	16	NM	NM
G292E		0.12Al	5.06	890	33	2.01	0.92	0.59	1.43	10	1500/5	16	.0001	15.2
G292F		0.12Al	5.02	890	35	2.01	0.90	0.60	1.51	NM	1500/5	16	NM	NM
G302-2C	0.15Gd	0.10Al	5.24	865	60	2.02	0.88	0.73	1.92	15	1500/5	24	.0001	15.6
G302-2A	0.15Gd	0.10Al	5.26	844	55	2.02	0.87	1.19	3.03	8	1475/5	24	.0001	15.6
G302F	0.15Gd	0.10Al	5.26	825	60	2.02	0.89	0.73	1.92	12	1500/5	16	NM	NM
G334C	0.50Gd	0.02Al	5.76	815	155	2.04	0.73	1.90	4.85	10	1475/5	24	.0001	16.3
G334A	0.50Gd	0.02Al	5.75	NM	NM	NM	0.79	1.04	3.04	18	1500/5	24	.0004	16.2
G302E	0.15Gd	0.10Al	5.23	810	70	2.02	0.90	0.72	1.86	13	1500/15	16	.0001	15.5
G298-2A	0.60Gd		5.89	805	190	2.05	0.70	2.39	5.77	11	1475/5	24	NM	NM
G302C	0.15Gd	0.10Al	5.28	900	52	2.02	0.86	1.03	2.50	8	1475/5	16	NM	NM
G298-2C	0.60Gd		5.84	770	207	2.05	0.65	1.95	5.21	18	1500/5	24	.0001	16.4
G298C	0.60Gd		5.85	750	200	2.06	0.66	2.01	4.52	16	1475/5	16	NM	NM
G331A	0.30Gd	0.08Al	5.47	745	95	2.03	0.83	1.19	2.58	13	1475/5	24	.0001	15.8
G331C	0.30Gd	0.08Al	5.42	NM	NM	NM	0.86	0.79	2.15	20	1500/5	24	.0001	15.8
G293F		0.15Al	5.05	710	33	2.01	0.90	0.63	1.52	NM	1500/5	16	NM	NM
G293C		0.15Al	5.03	700	34	2.01	0.90	0.71	1.65	8	1500/5	16	NM	NM
G293E		0.15Al	5.01	690	36	2.01	0.89	0.60	1.50	NM	1500/5	16	NM	NM
G335C	0.50Gd	0.04Al	5.72	680	170	2.05	0.82	1.85	4.78	10	1475/5	24	.0001	16.0
G335A	0.50Gd	0.04Al	5.72	NM	NM	NM	0.86	1.04	2.84	23	1500/5	24	.0001	16.0
G303-2C	0.15Gd	0.15Al	5.24	572	76	2.03	0.87	0.92	1.88	14	1500/5	24	.0001	15.2
G303-2A	0.15Gd	0.15Al	5.27	570	78	2.03	0.86	1.47	3.53	7	1475/5	24	.0001	15.2
G329A	0.30Gd	0.10Ga	5.58	550	125	2.04	0.87	1.43	3.12	11	1475/5	24	.0001	15.9
G329D	0.30Gd	0.10Ga	5.55	NM	NM	NM	0.87	1.04	2.69	13	1500/5	24	.0001	15.9
G303C	0.15Gd	0.15Al	5.23	500	73	2.03	0.85	1.57	3.34	6	1475/5	16	NM	NM
G332C	0.30Gd	0.12Al	5.45	495	140	2.04	0.84	1.46	3.43	11	1475/5	24	.0001	15.7

Table I. Compositions Prepared and Evaluated (continued)

$$3\left[(1-x)\,Y_2O_3 \cdot x\,RE_2O_3\right] \cdot 5\left[(1-w)\,F^a_{1.925}O_3 \cdot w\,T^1_{1.925}O_3\right]$$

SMEC No.	Composition x	X	w	Density gm/cm²	4πMs (gauss) 25°C	ΔH(oe) (x Band)(25°C)	Batt Factor	Remanence Ratio (Rg) 60~, 25°C	Coercive Feel H₀,Koe 60~, 25°C	Drive Field (H_d) (oe)	Particle Size Microns	Firing Temp °C/hr	Waxing Time Hrs	Loss Tangent x Band	Dielectric Constant(€) x Band
G332E	0.30Gd		0.12Al	5.43	NM	NM	NM	0.84	1.03	2.81	16	1500/5	24	.0001	15.7
G303E	0.15Gd		0.15Al	5.21	495	92	2.03	0.90	0.91	2.51	NM	1500/16	16	NM	NM
G303F	0.15Gd		0.15Al	5.24	485	80	2.03	0.90	1.03	2.64	NM	1500/5	16	NM	NM
G250-2C			0.25Al	4.90	300	40	2.03	0.85	1.18	2.10	NM	1475/5	16	NM	NM
G339B	0.30Gd	0.05Dy	0.15Al	NM	285	NM	NM	0.93	2.13	3.97	NM	1475/5	24	.0001	15.5
G336C	0.50Gd		0.10Al	5.72	280	305	2.11	-	High	-	9	1475/5	24	.0001	15.9
G356A	0.50Gd		0.10Al	5.73	NM	NM	NM	0.88	1.86	3.98	19	1500/5	24	NM	NM
G340B	0.30Gd	0.04Dy	0.15Al	NM	277	NM	NM	0.91	2.18	3.84	NM	1475/5	24	.0001	15.5
G294C	1.0Gd			6.32	90	NM	NM	Unable To Measure	-	-	22	1475/5	16	NM	NM

BLANK PAGE

$$3\left[0.85Y_2O_3 \cdot 0.15Gd_2O_3\right] \cdot 5\left[0.95Fe_{1.925}O_3 \cdot 0.05A\ell_{1.925}O_3\right]$$
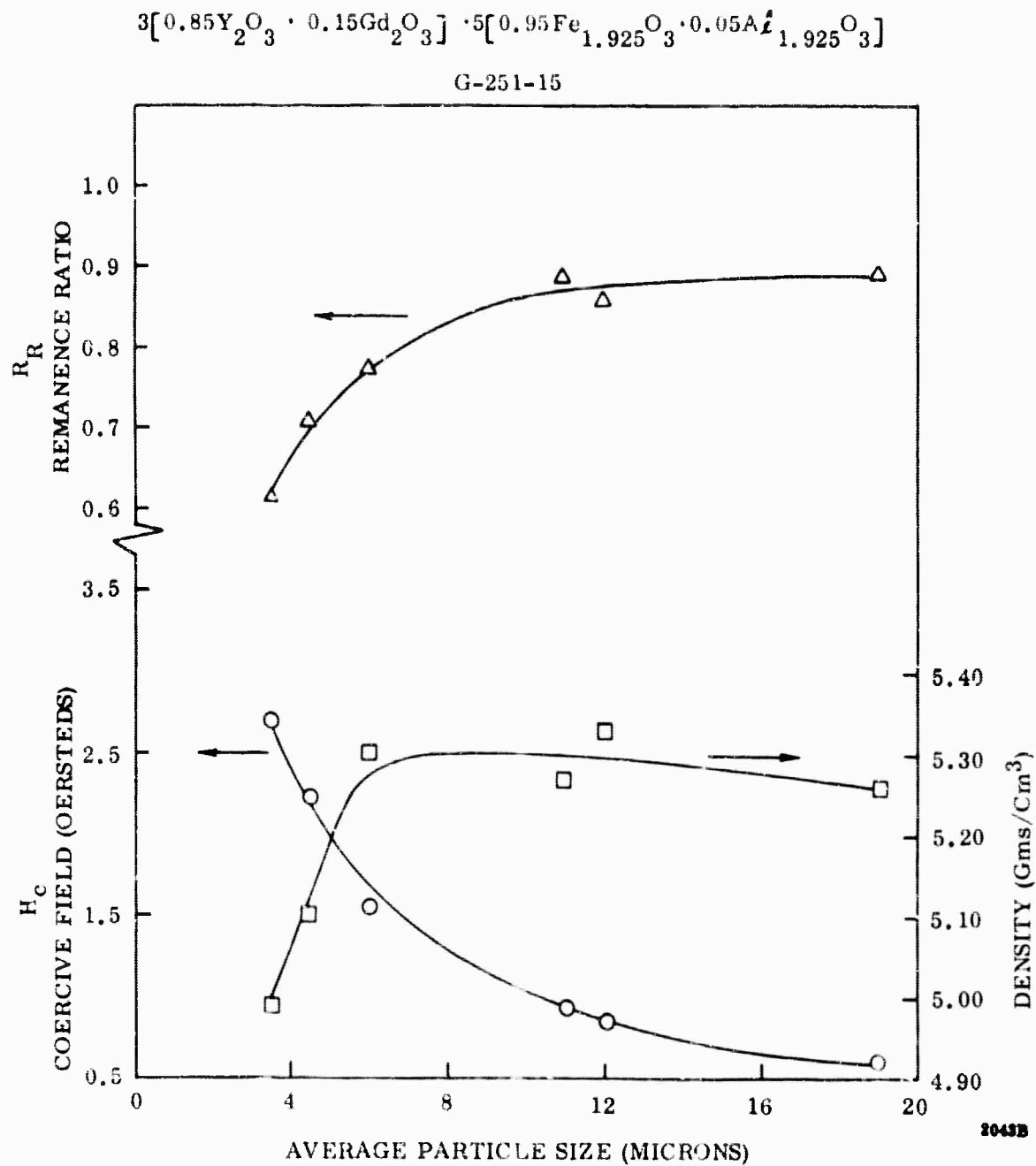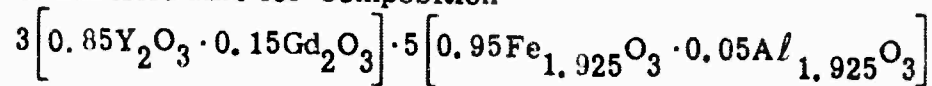
G-251-15

Figure 23. Coercive Field, Remanence Ratio and Density as a Function of Particle Size for Composition

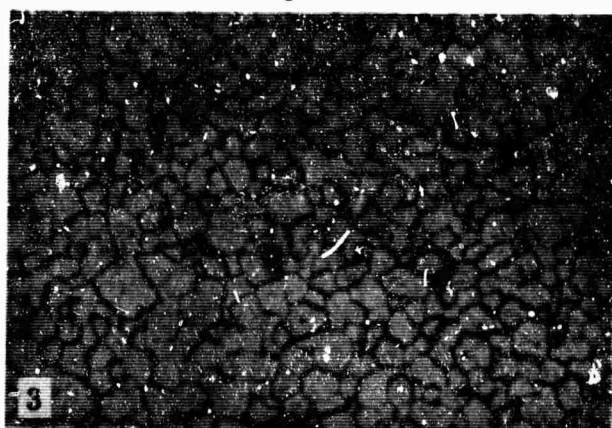$$3\left[0.85Y_2O_3 \cdot 0.15Gd_2O_3\right] \cdot 5\left[0.95Fe_{1.925}O_3 \cdot 0.05A\ell_{1.925}O_3\right]$$

4-21

$$3\left[85\%Y_2O_3 \cdot 15\%Gd_2O_3\right] \cdot 5\left[95\%Fe_{1.925}O_3 \cdot 5\%A\ell_{1.925}O_3\right]$$
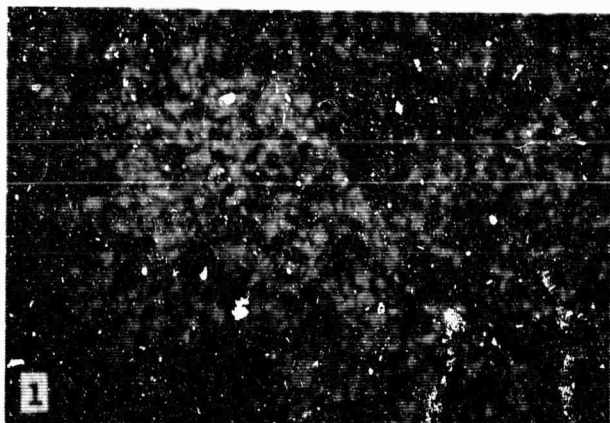
G-251-15Y
Avg. Particle Size 3 to 4 Microns
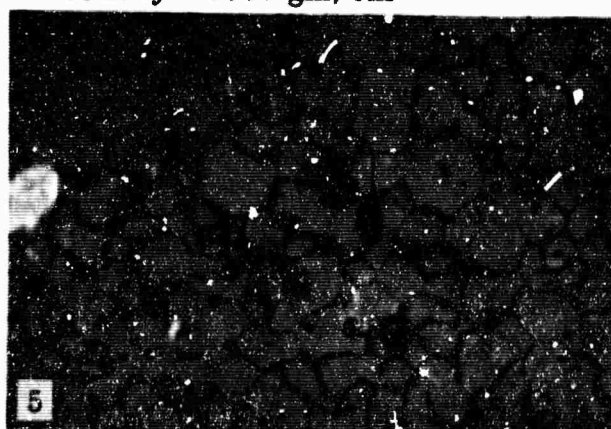Density = 4.99 gm/cm^3
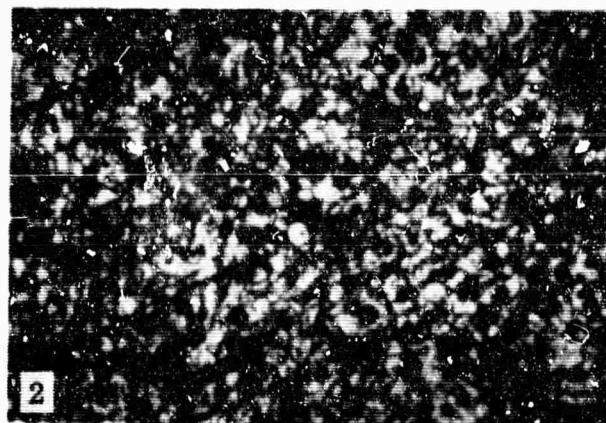
G-251-15W
Avg. Particle Size 4 to 5 Microns
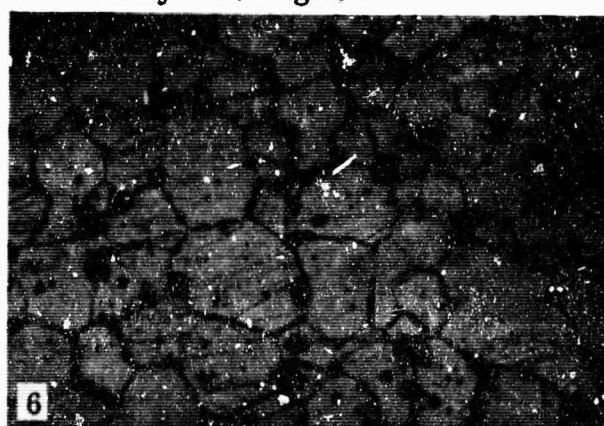Density = 5.10 gm/cm^3

G-251-15S
Avg. Particle Size 6 Microns
Density = 5.30 gm/cm^3

G-251-15V
Avg. Particle Size 11 Microns
Density = 5.27 gm/cm^3

G-251-15T
Avg. Particle Size 12 Microns
Density = 5.33 gm/cm^3

G-251-15R
Avg. Particle Size 19 Microns
Density = 5.26 gm/cm^3

1024P

Figure 24.   Grain Size Photograph of the Yttrium Gadolinium Aluminum Iron
Garnets (G-251) of Figure 21 and Table II.

Similar data are presented for the composition of 30 percent gadolinium substituted yttrium iron garnet (G-296C, G-296-3C, and G-296-2C of Table I) in Figure 25. By increasing the ball milling time to 24 hours, thereby increasing the grain size of the material to around 22 microns, the remanence ratios were increased from 0.65 to 0.9 and the coercive fields were reduced from 1.2 oersteds to approximately 0.7 oersted. This technique can be used and has been used on nearly all compositions to improve the square loop properties of the material.

These data indicated that each composition may require an optimum particle size rather than a given particle size which is acceptable for all compositions. In all cases, the coercive field decreases and remanence ratio increases with increasing particle size. In one composition an average particle size of 12 microns or greater may be desired (as illustrated in Figure 23) while in others a particle size greater than 20 microns may be required for optimum characteristics (as in Figure 25). Additional experiments are under way to more thoroughly investigate and evaluate these grain size effects.

Hysteresis Properties Of The Yttrium Gadolinium Aluminum Iron Garnets.
Since these materials are of particular interest due to their temperature-compensated magnetization, additional data are presented on the hysteresis properties of these compounds in graphical profile form.

The data obtained on yttrium gadolinium iron garnet (See Figure 17) are presented in Figure 26. Most of the compositions were prepared using a ball milling time (presintered oxide stage) of 16 hours. This is not the optimum time for many of these compositions as illustrated for the gadolinium content of $x = 0.30$ (See G-296 in Figure 25). Here a noted decrease in coercive field and increase in remanence ratio are obtained by increasing the ball milling time to 24 hours. However, there is noted a general intrinsic increase (not particularly severe) in coercive field with gadolinium content. This is attributed to the increase in the anisotropy field (or linewidth) as the gadolinium content is increased.
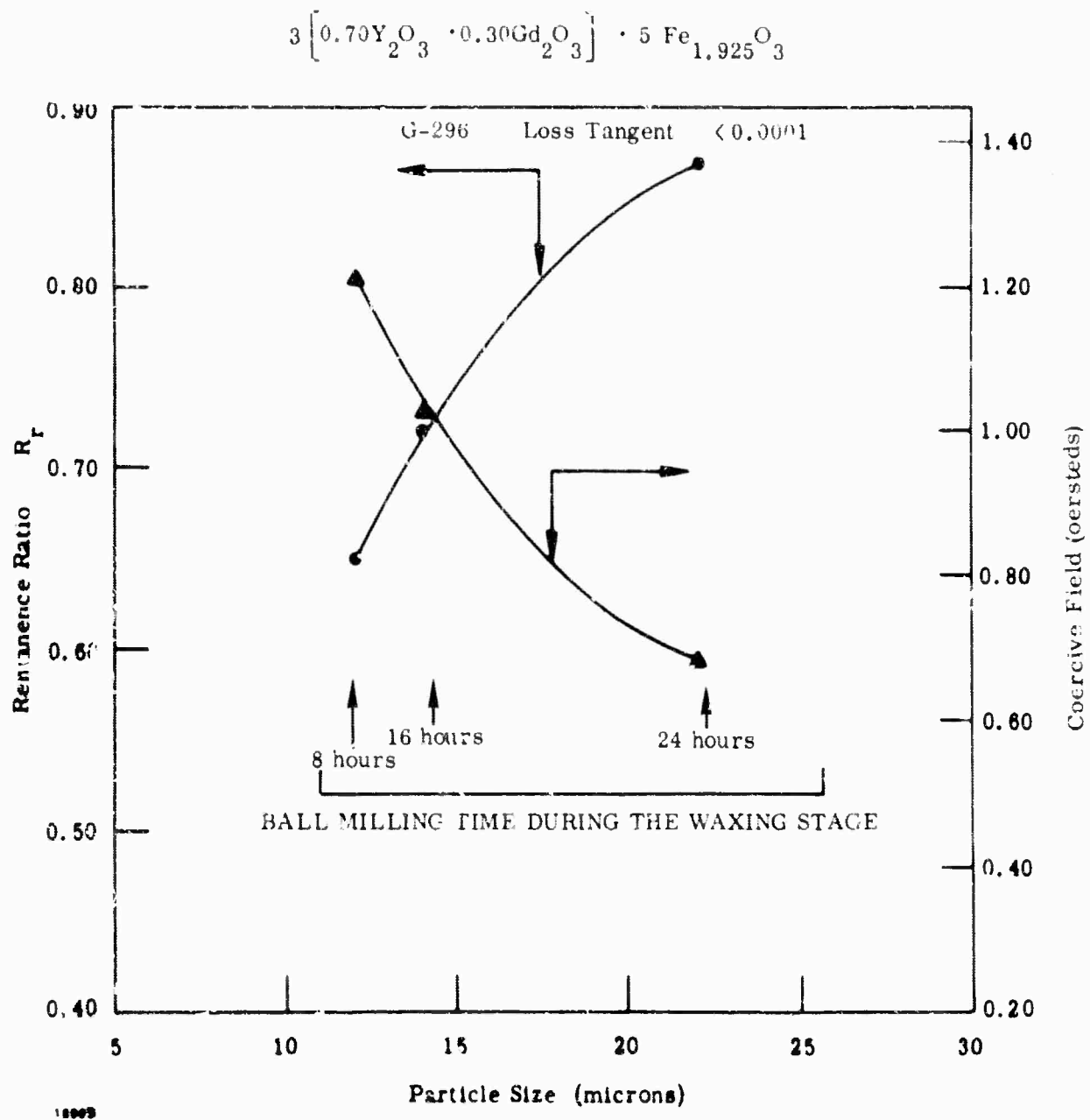
$$3 \left[0.70 Y_2 O_3 \cdot 0.30 Gd_2 O_3 \right] \cdot 5\ Fe_{1.925} O_3$$

Figure 25. Remanence Ratio and Coercive Field Vs Particle Size in
$3 \left[0.70 Y_2 O_3 \cdot 0.30\ Gd_2 O_3 \right] \cdot 5\ Fe_{1.925} O_3$

$$3\left[(1-x)Y_2O_3 \cdot xGd_2O_3\right] \cdot 5Fe_{1.925}O_3$$
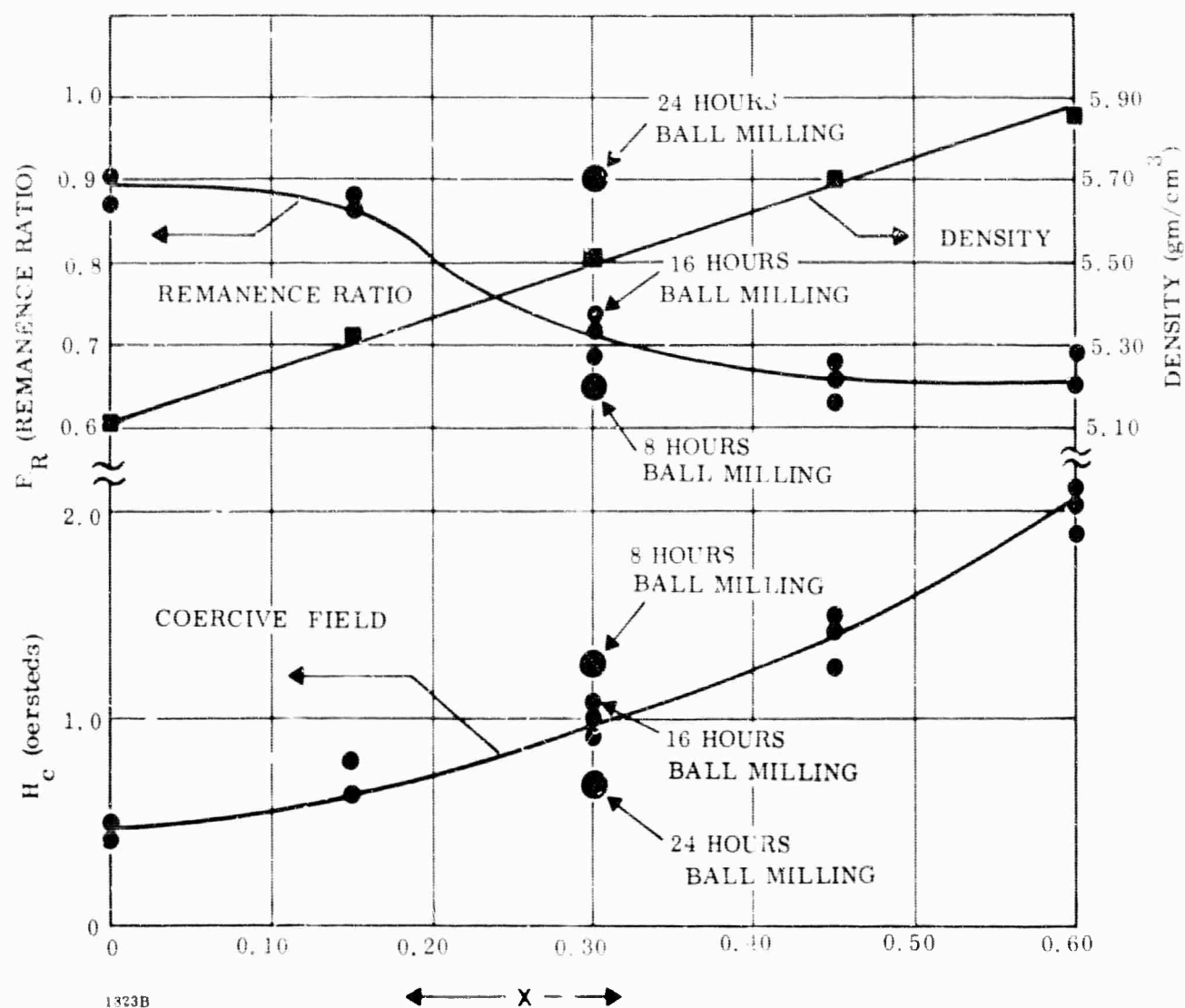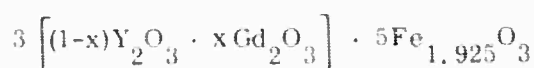

Figure 26. Remanence ratio, coercive field, and density of yttrium
gadolinium iron garnet as a function of gadolinium content

The data obtained on the yttrium aluminum iron garnet compositions are pre-
sented in Figure 27. In these materials the coercive field is observed to increase with
aluminum content. This does not seem to be an intrinsic characteristic but seems to
be due primarily to the fact that particle size decreases as more aluminum is substi-
tuted into the sample. Aluminum oxide is a highly refractory material and thus higher
firing temperatures are required for larger substitutions of aluminum. The coercive
field is observed to decrease when the firing temperature is increased from $1475^{\circ}C$ to
$1500^{\circ}C$. These compositions are G-289 (x=0), G-290 (x=0.03), G-291 (x=0.08),
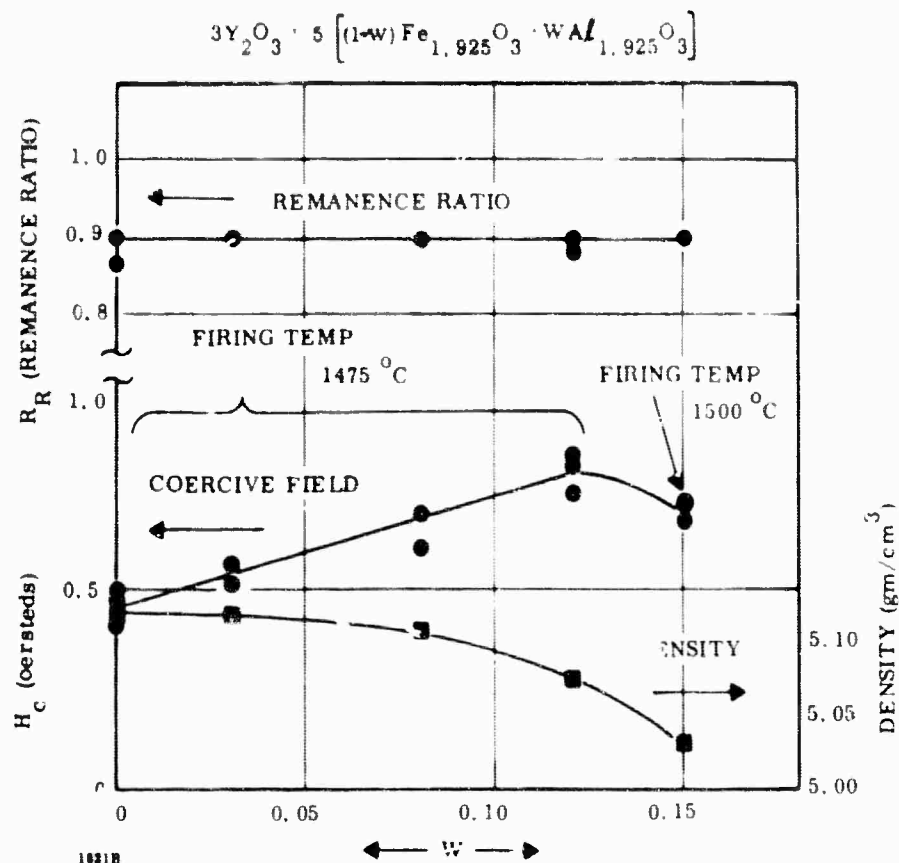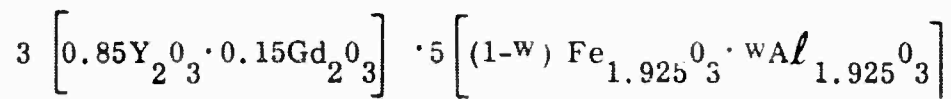G-292 (x=0.12), and G-293 (x=0.15) as listed in Table I.

Figure 27. Remanence ratio, coercive field, and density of yttrium aluminum iron garnet as a function of aluminum content

The characteristics of one particular series of yttrium gadolinium aluminum iron garnet family of materials namely

$$3 \left[0.85 Y_2 O_3 \cdot 0.15 Gd_2 O_3 \right] \cdot 5 \left[(1-w) Fe_{1.925} O_3 \cdot wA\ell_{1.925} O_3 \right]$$

are presented in Figure 28. See Figure 18 for the $4\pi M_s$ as a function of temperature for these materials.
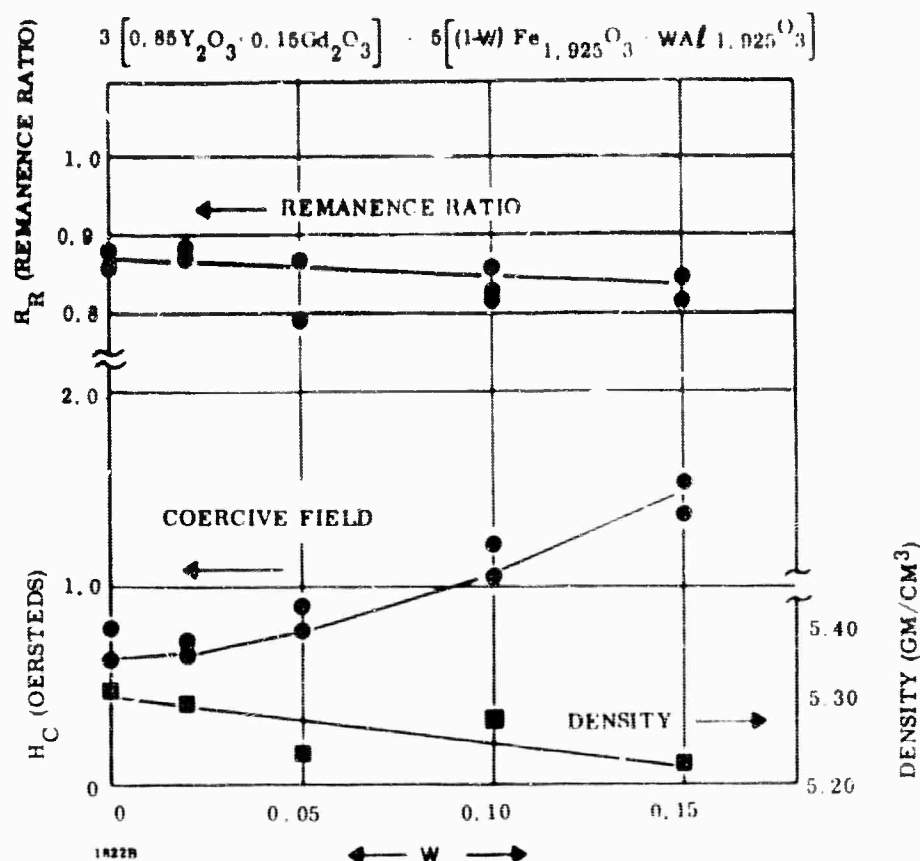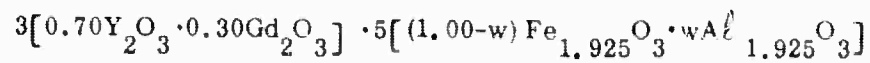
Figure 28. Remanence ratio, coercive field, and density of yttrium gadolinium aluminum iron garnet as a function of aluminum content

Figure 29 presents graphically the data collected on the compositions,

$$3 \left[0.70 \, Y_2O_3 \cdot 0.30 \, Gd_2O_3 \right] \cdot 5 \left[(1-w) Fe_{1.925} \cdot wAl_{1.925}O_3 \right]$$ for two different firing temperatures. (See Figure 21 for temperature characteristics.) Linewidth (ΔH), magnetization ($4\pi M_s$), coercive field (H_c), and remanence ratio (R_R) are presented as a function of the compositional parameter w (aluminum content). The linewidths and magnetization obtained for the firing temperature of 1500°C are not significantly different from those obtained at 1475°C. A significant decrease in coercive field is noted for material prepared at the higher firing temperature. The coercive field

$$3\left[0.70Y_2O_3 \cdot 0.30Gd_2O_3\right] \cdot 5\left[(1.00-w)Fe_{1.925}O_3 \cdot wA\ell_{1.925}O_3\right]$$

$0.83 \leq R_R \leq 0.90$ (FOR ALL COMPOSITIONS) (R_R = REMANENCE RATIO)

LOSS TANGENT < 0.0001

DIELECTRIC CONSTANT $\doteq$ 15.8

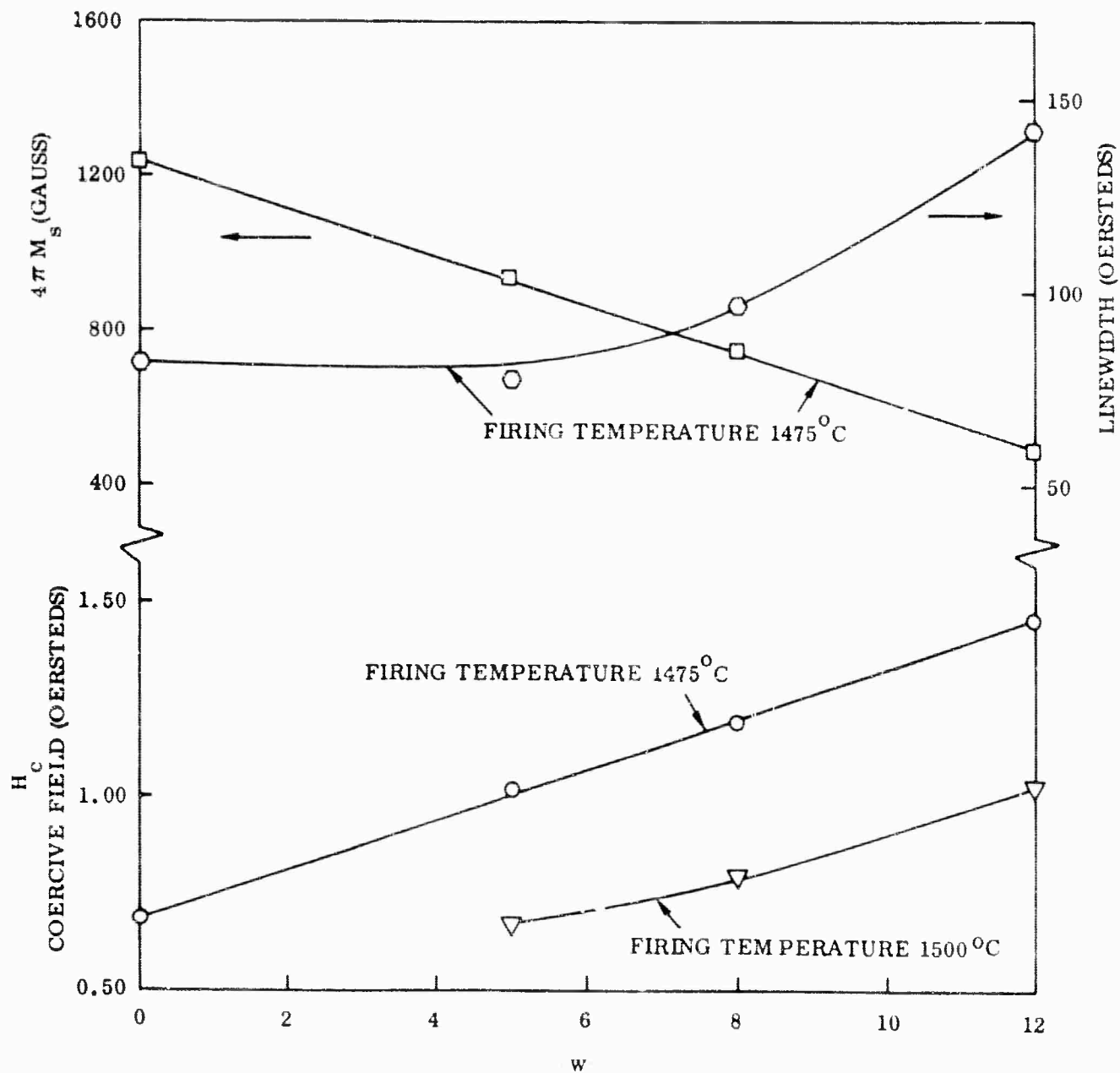Figure 29. Linewidth, Magnetization, Coercive Field, and Remanence Ratio
as a Function of Aluminum Content in

30443 $\qquad 3\left[0.70Y_2O_3 \cdot 0.30Gd_2O_3\right] \cdot 5\left[(1-w)Fe_{1.925}O_3 \cdot wA\ell_{1.925}O_3\right]$
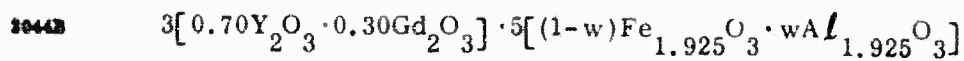
increases with aluminum content in much the same fashion as linewidth. The noted decrease in coercive field with firing temperature is attributed to the larger grain growth for the 1500°C firing temperature. The apparent intrinsic increase in coercive field as a function of aluminum content is most likely due to the increase in anisotropy field of the material (anisotropy field is proportional to the linewidth in these materials.) These data are very similar to that observed for $3\left[0.85\ Y_2 0_3\right.$ $\left.\cdot 0.15\ Gd_2 0_3\right]\cdot 5\left[(1-w)Fe_{1.925}0_3\cdot wAl_{1.925}0_3\right]$ of Figure 27.

Rare Earth Substitutions. Compositions composed of small substitutions (5 to 10%) of dysprosium, holmium, ytterbium, erbium and samarium for yttrium in yttrium iron garnet were prepared. In general, the coercive field was observed to increase slightly with rare earth content, but no significant changes in remanence ratio were observed. The various compositions prepared are listed in Table I.

Temperatu Measurements. Coercive fields have been measured for many of the compositions as a function of temperature. Typical data are presented for the yttrium gadolinium, the yttrium aluminum, and the 85% yttrium -15% gadolinium aluminum iron garnet families in Figures 30, 31, and 32 respectively.

The coercive field decreases with increasing temperature in all compositions studied. The amount of decrease appears proportional to the decrease in anisotropy field (or linewidth) with temperature; that is, the greater the decrease in anisotropy field with temperature, the greater the decrease in coercive field. The temperature sensitivity of the anisotropy field is dependent on the composition. Typically, the decrease in coercive field over a temperature range of 10°C to 110°C is 25% to 50% depending on the composition.

Remanence ratios $\left(\dfrac{4\pi M_R}{4\pi M_s}\right)$ have not been observed to be temperature sensitive. However, this does not mean that the remanent magnetization $(4\pi M_R)$ is not temperature sensitive in some compositions. The phase shift in a device is proportional to the value of $4\pi M_R$, so it is important to measure the temperature dependence of the $4\pi M_R$ and/or the $4\pi M_s$ independently to give a true picture of the temperature stability of the material. Some of the data on $4\pi M_s$ versus temperature for the yttrium gadolinium aluminum iron garnets have been presented in
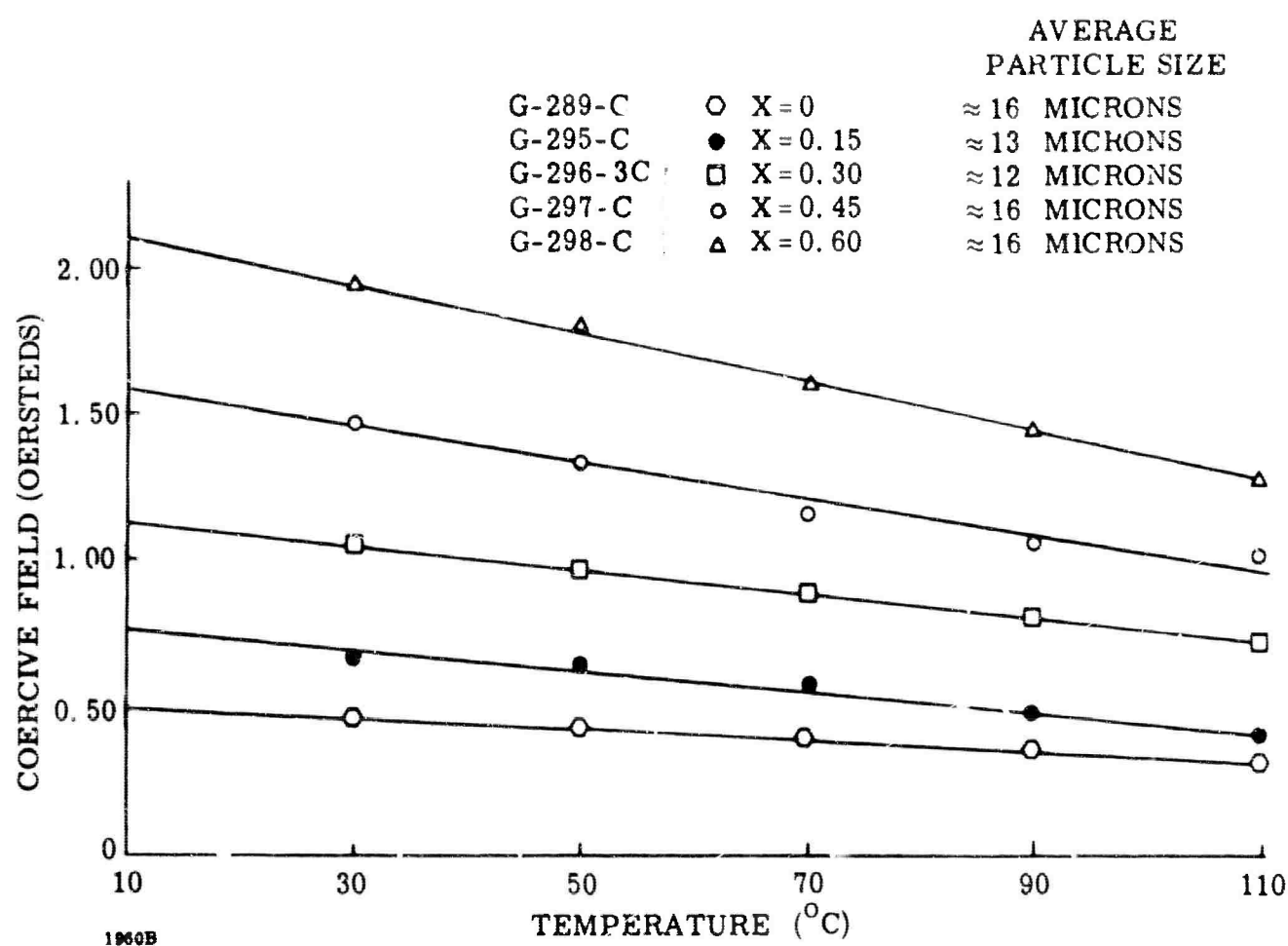
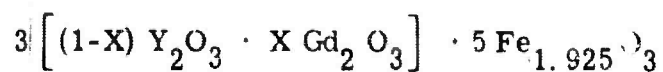$$3\left[(1-X)\ Y_2O_3\ \cdot\ X\ Gd_2\ O_3\right]\ \cdot\ 5\ Fe_{1.925}\ )_3$$

Figure 30. Coercive Field as a Function of Temperature for the
Yttrium Gadolinium Iron Garnet Compositions

$$3\ Y_2O_3 \cdot 5 \left[(1-w)\ Fe_{1.925}O_3 \cdot wA\ell_{1.925}O_3\right]$$

AVERAGE
PARTICLE SIZE

G-289-C	○ W = 0	≈ 16	MICRONS
G-290-D	● W = 0.03	≈ 16	MICRONS
G-291-D	□ W = 0.08	≈ 8	MICRONS
G-292-C	△ W = 0.12	≈ 6	MICRONS
G-293-D	○ W = 0.15	≈ 8	MICRONS

COERCIVE FIELD (OERSTEDS)
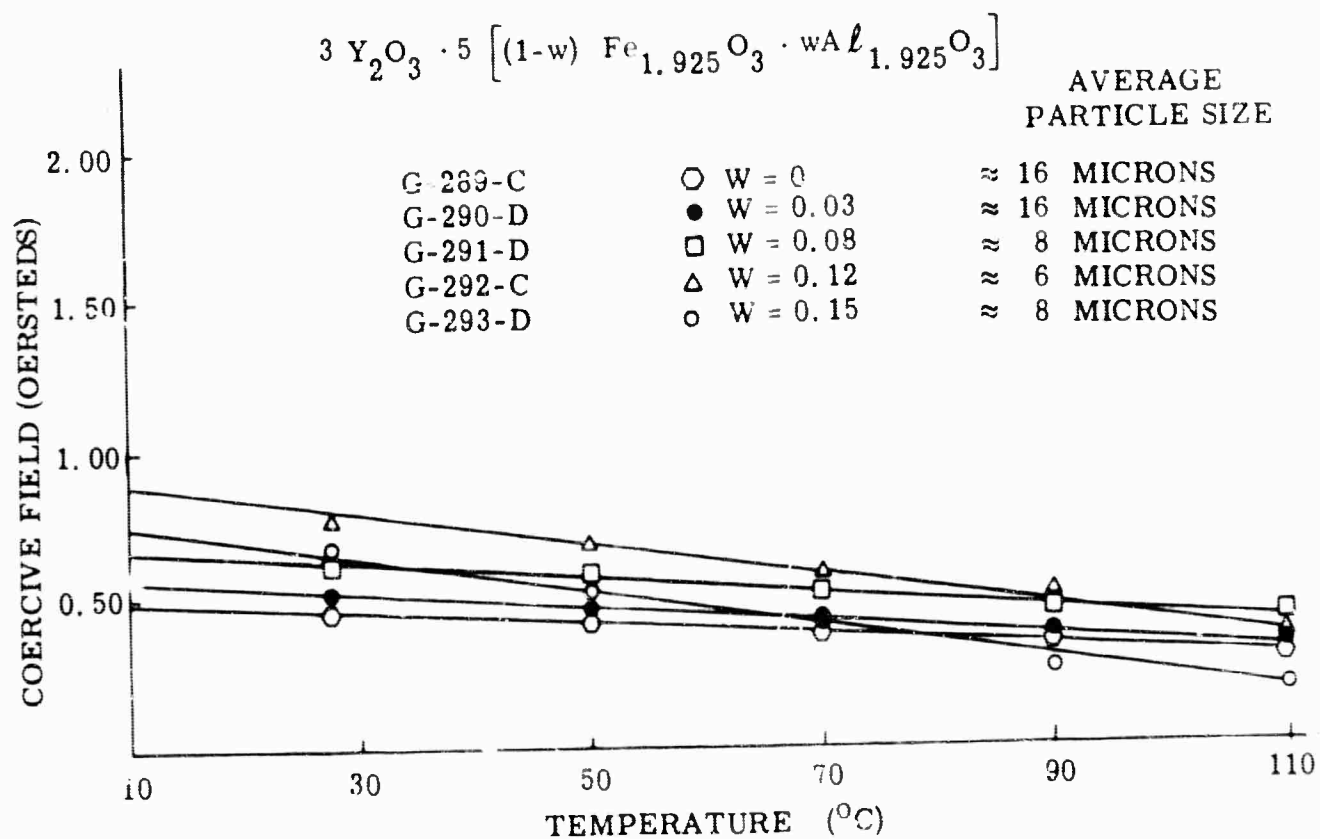
TEMPERATURE (°C)

1951B

Figure 31. Coercive Field as a Function of Temperature for the
Yttrium Aluminum Iron Garnet Compositions

4-31

$$3 \left[0.85 \text{ Y}_2\text{O}_3 \quad \cdot \quad 0.15 \text{ Gd}_2\text{O}_3 \right] \quad \cdot \quad 5 \left[(1\text{-w}) \text{ Fe}_{1.925}\text{O}_3 \quad \cdot \text{wA}\ell_{1.925}\text{O}_3 \right]$$

AVERAGE
PARTICLE SIZE

G-289-C	◐	W = 0	≈ 16 MICRONS
G-301-C	●	W = 0.02	≈ 13 MICRONS
G-251-9U	□	W = 0.05	≈ 18 MICRONS
G-302-C	○	W = 0.10	≈ 8 MICRONS
G-303-C	△	W = 0.15	≈ 6 MICRONS
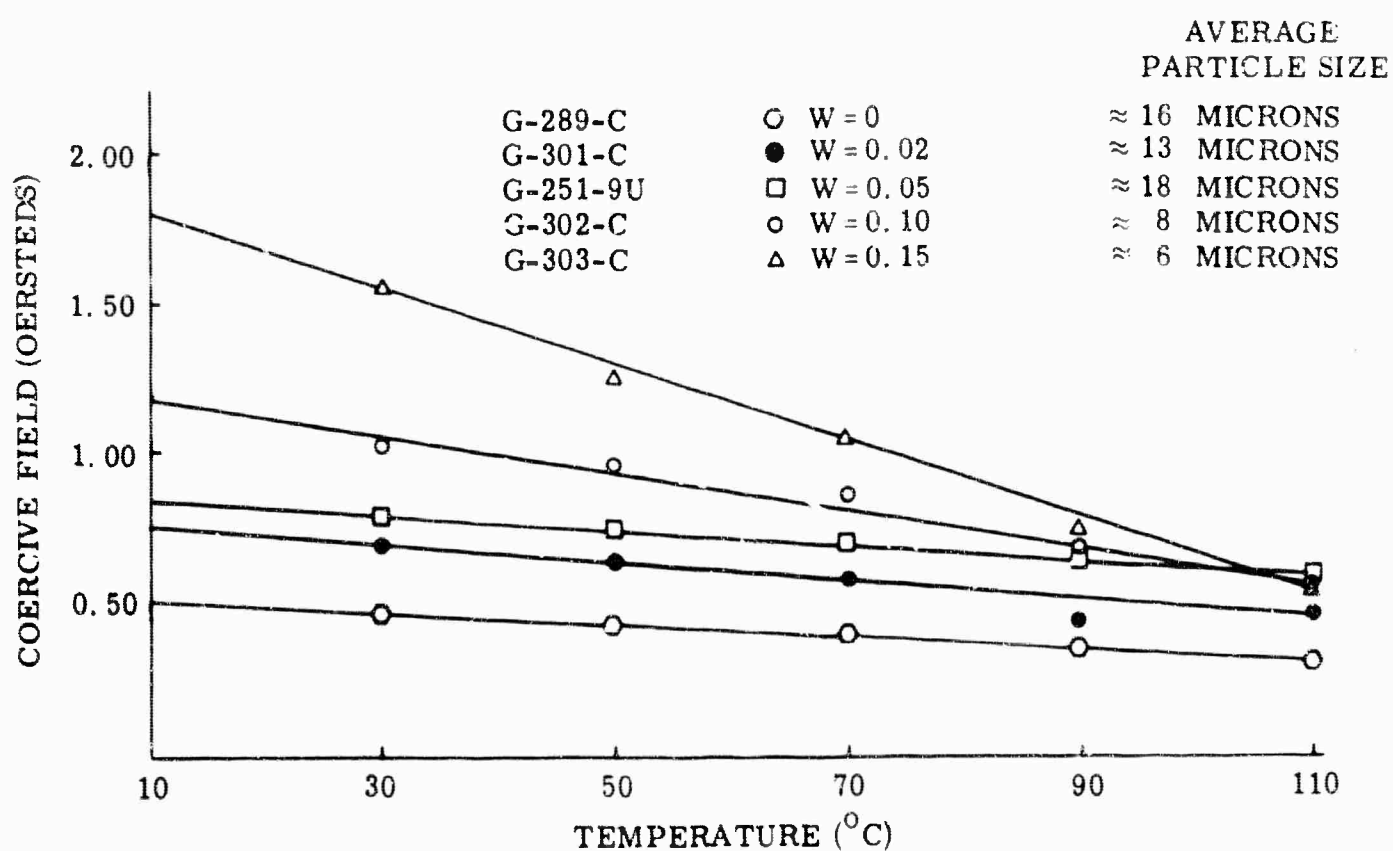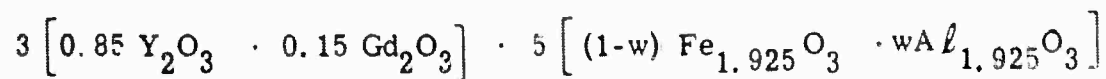
1959B

Figure 32. Coercive Field as a Function of Temperature for the
85% Yttrium 15% Gadolinium Aluminum Iron Garnet
Compositions

Figure 17 to 22. These materials exhibit equally good temperature stability of the remanent magnetization. Additional experiments are presently being performed on these parameters.

Conclusions. The data obtained on the many garnet compositions studied indicate the following conclusions:

1. The coercive field and the remanence ratio are a strong function of grain size of the material. The larger the grain size the lower the coercive field and the higher the remanence.

2. The grain size of any particular composition can be controlled by the ball milling time of the presintered oxides. The longer the ball milling time the larger the grain size in the final fired ceramic. (However, the ball milling time cannot exceed that which alters the desired microwave characteristics, such as increasing the dielectric loss tangent.) The optimum grain size will be different for each composition; however, grain sizes in the 15 to 25 micron range seem desirable.

3. The coercive field and remanence ratio do not seem to be a strong function of composition. These parameters seem to be controlled primarily by the preparation procedures rather than by composition. There is, however, some variation in coercive field noted as a function of composition. These variations seem to be related to the rare earth content of the materials. This is probably due to the fact that the anisotropy field in garnets is primarily dependent on the rare earth content (ion located on 24c lattice site) and the coercive field will certainly be influenced to a degree by the anisotropy field. Some variation in coercive field as a function of composition is anticipated therefore when the rare earth ions are being changed.

4. The remanence ratios measured on essentially all samples are in the 0.80 to 0.90 area. In some cases these values were not obtained on the first samples, but by varying the ball milling time (and thus increasing the grain size in the final fired ceramic) in the preparation procedure, the remanence ratios improved to these values.

5. The coercive fields of these compositions exhibit more compositional dependence than remanence ratios. The coercive fields vary from about 0.4 oersted upto a little greater than 2 oersteds. However, the data indicate that most compositions can be made with coercive fields less than 1 oersted. Ball milling time in the preparation procedure again seems to be the controlling parameter.

6. It is noted from the data that as the compositions are substituted with large amounts of aluminum, the coercive fields seem to increase. This is due primarily to the fact that particle size decreases as more aluminum is substituted into the sample. Aluminum oxide is a highly refractory material and thus higher firing temperatures are required for growth of larger grains. When the firing temperatures were increased from $1475^{\circ}C$ to $1500^{\circ}C$, coercive fields were reduced from a maximum of approximately 0.85 oersted to around 0.65 oersted.

7. It is noted that the compositions listed in Table I give a very large range in values of $4\pi M_s$. This is important in covering the entire frequency range from L band through X band. Many of these compositions also possess temperature stability of the magnetization. In particular, the yttrium gadolinium iron and the yttrium gadolinium aluminum iron garnets exhibit temperature compensation of the magnetization which is important in deriving temperature insensitive phase shifters. Some data have been obtained on the temperature dependence of the remanence magnetization and this seems to be as good, and in some cases better, than the temperature stability of the saturated value of the magnetization.

8. Microwave power measurements indicate that the rare earth substituted garnets show increased rf peak power thresholds. Some of the holmium and dysprosium substituted YIG compositions have peak power thresholds in the 100 kw area. This is very comparable to similar measurements on equivalent compositions made in conventional microwave structures where a dc magnetic biasing field is required.

9. Rare earth substitutions can be made to improve peak power thresholds without severly altering the hysteresis properties of this material.

4.3.4 RF Structure Evaluations

A waveguide test housing has been fabricated in WR-112 waveguide (X band) for use in material evaluation. A study is currently under way to determine a toroidal geometry which will be generally useful in correlating microwave properties with the measured material parameters.

It is expected that the optimum geometry established for the materials presently under test will also be optimum for most other materials.

Design techniques have also been established for matching into the ferrite loaded waveguide and maintaining VSWR under 1.25. The use of quarter wavelength dielectric steps has been found to be the most convenient means of achieving this.

Test structures are also being fabricated in TEM mode transmission lines to evaluate toroidal geometries at lower frequencies in the L-band region. This is a slab line test piece and was designed to accommodate many of the toroids made for X band and thus make duplicate use of as many materials as possible. Microwave measurements for material evaluation will be made in these structures during the next quarter.

It is of interest to note that many of the materials maintain a good square loop property even though the toroids are "pieced" together. That is, a square toroid can be constructed out of two U-shaped pieces of ferrite and still maintain a good remanence ratio and a low coercive field. This is valuable information in studying device structures because it simplifies the material geometry and in many cases reduces the cost of machining materials for microwave evaluation. The finishes required on the jointing surfaces are those obtained in normal ferrite grinding procedures. Remanence ratios of 0.8 to 0.85 have been obtained for toroids in this type of configuration.

Specific device efforts to date have been chiefly concerned with increasing the ratio of phase shift to loss at X band using a material possessing high peak power capability. The most promising material used to date is G-286 having the composition $3 (0.02DY_2O_3 \cdot 0.98Y_2O_3) \cdot 5 (0.92Fe_{1.925}O_3 \cdot 0.08Al_{1.925}O_3)$, $4\pi M_s = 1115$ gauss, linewidth = 81 oersteds, remanence ratio = 0.87, and coercive force = 0.70 oersted. The hysteresis curve for this material is shown in Figure 33. Figure 34 shows a cross-sectional view of the most recent, empirically derived material configuration for the X-band waveguide phase shifter.

Testing in the 8500-9500 mc range yielded the following results at low power levels and room temperatures: VSWR = 1.20 maximum, loss = 0.25 db/inch, and differential phase shift = 90 degrees/inch. This configuration was also tested at high power levels and exhibited no high peak power effects up to the 70 kw power

level tested. To achieve the high peak power threshold, this material has both dysprosium doping and a value of $\omega_m/\omega < 0.4$. Switching data indicate that a four-bit phase shifter using this configuration would require 550 μjoules energy from the driver and would switch in 1μsec or less.

Investigations in the device area have revealed that toroided geometry using a smaller core width (less than the present 0.074") should yield improved performance These investigations will be continued during the next reporting period.
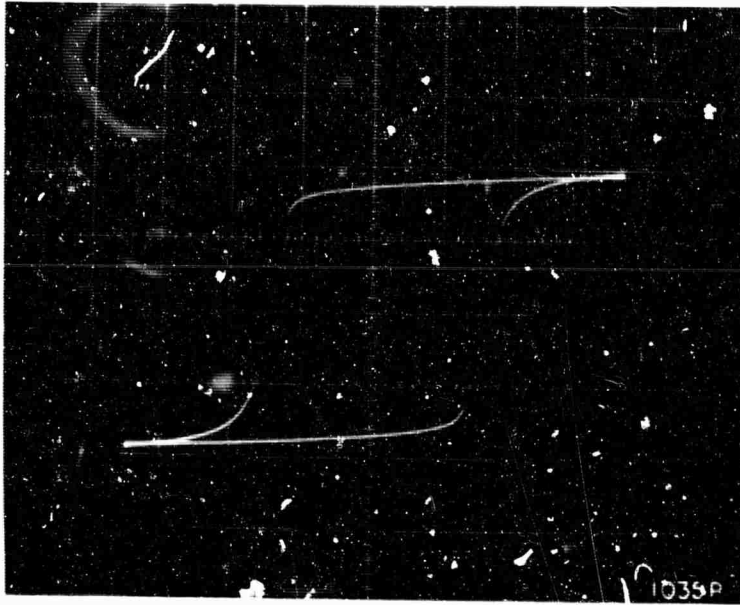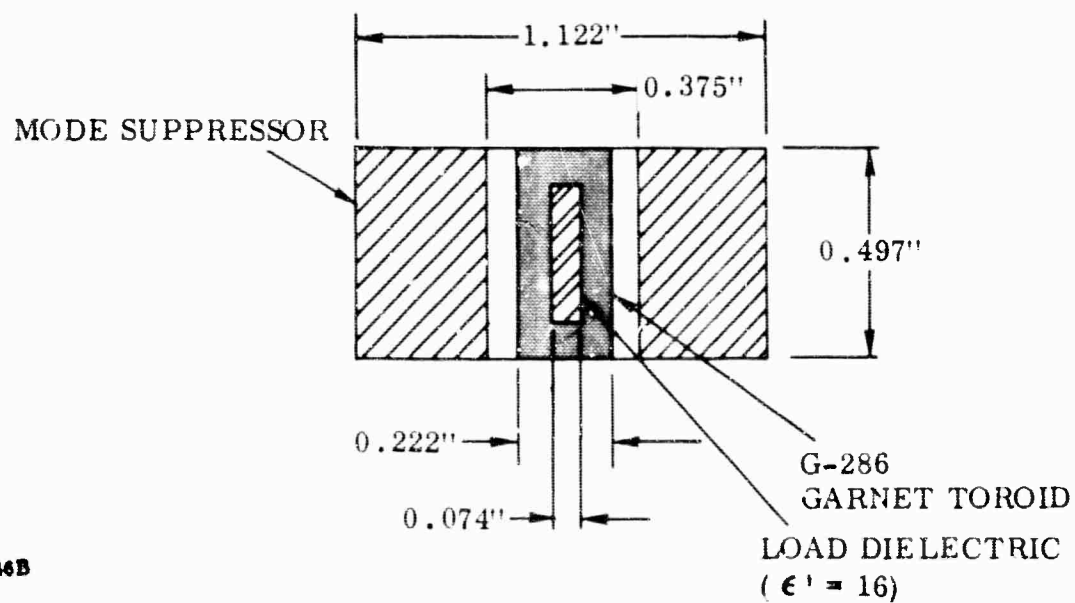
Figure 33. Hysteresis Loop for G-286

Figure 34. Cross-Sectional View of X-Band Digital Phase Shifters. Not Shown are cooling Channels, Charging Circuitry and Drivers.

5. PROGRAM PLANS FOR NEXT SEMIANNUAL PERIOD

The following investigations are planned for the next semiannual period:

1. Study of the effects of magnetostriction on coercive field and remanence ratio.

2. Study of the temperature stability of the coercive field and remanence ratio.

3. Study of strain relief in machined toroids by heat treatment to improve remanence ratios and coercive fields.

4. Continue the study and interpretation of grain size effects on hysteresis properties.

5. Begin investigation and evaluation of ferrite compositions.

6. Continue the evaluation of materials in the X-band waveguide test structure.

7. Begin similar evaluations in the L-band coaxial structure.

CUSTOMER	COPIES
General Electric Company ATTN: Mr. Hugh Hair Electronics Laboratory Building No. 3 Electronics Park Syracuse, New York	1
Advanced Technology Corporation ATTN: Mr. M. Cohen 1830 York Road Timonium, Maryland	1
Western Microwave Laboratory, Inc. ATTN: Mr. T. Giesler 1045 DiGiulio Avenue Santa Clara, California	1

DISTRIBUTION LIST

CUSTOMER	COPIES
ARPA The Pentagon Wash DC 20301	4
RTD (RTTG) Bolling AFB DC 20332	1
Battelle Memorial Institute ATTN: Security Officer 505 King Avenue Columbus 1, Ohio	2
DDC (TISIA-2) Cameron Stn Alexandria Va 22314	20
RADC (EMATE/Mr. P. A. Romanelli) Griffiss AFB NY 13442	4
Advisory Group on Electron Devices ATTN: Mr. W. Kramer 346 Broadway New York, New York 10013	2
Westinghouse Electric Corporation ATTN: Mr. G. S. Blevins) Electronic Division P. O. Box 1897 Baltimore 3, Maryland	1
The Bendix Corporation Bendix Radio Division ATTN: Mr. G. Engelbert Department No. 481 Towson 4, Maryland	1
Hughes Aircraft Company ATTN: Mr. Robert A Moore Building 600 P.O. Box 3310 Fullerton, California 92634	1